Journal of Pharmaceutical Innovation (2026) 21:521
https://doi.org/10.1007/s12247-026-10752-2

RESEARCH

Development and Characterization of Herbal Extract-Loaded Nanoemulgels for Periorbital Hyperpigmentation and Edema: Antioxidant, Anti-inflammatory, and Anti-tyrosinase Activities

Ebru Altuntaş[1] · Vildan Manav[2,3] · Merve Yılmaz[1] · Ayşe Esra Karadağ[4]

Received: 24 September 2025 / Accepted: 10 May 2026
© The Author(s) 2026

Abstract

Purpose Periorbital dark circles and edema are frequent cosmetic concerns that contribute to an older and fatigued appearance, thereby diminishing self-esteem and overall quality of life. Conventional topical regimens are often limited by the low stability, poor aqueous solubility, and insufficient epidermal penetration of many active compounds. To address these problems, we developed and characterized nanoemulgel (NEG) formulations utilizing standardized extracts of *Glycyrrhiza glabra (G. glabra*) and *Aesculus hippocastanum (A. hippocastanum*). These formulations were designed as multifunctional topical platforms with potential relevance to both pigmentation-related and edema-associated periorbital concerns.

Methods Oil-in-water nanoemulsions (NEs) were prepared by ultrasonication using Quillaja saponin alone or combined with Kolliphor® P188 and subsequently gelled with xanthan gum. Physicochemical properties (droplet size, polydispersity index (PDI), zeta potential, pH, viscosity, and conductivity) and stability were evaluated. Antioxidant (DPPH, ABTS), anti-inflammatory (lipoxygenase inhibition), and anti-tyrosinase activities were assessed.

Results Among the generated NEGs, two formulations exhibited distinct physicochemical profiles. The saponin-based formulation F3P2 exhibited a droplet size of 142.70 ± 1.90 nm, a PDI of 0.184 ± 0.01, and a markedly negative zeta potential of −59.0 ± 3.3 mV, signifying strong electrostatic stabilization. In contrast, the hybrid formulation F6P2, which integrates saponin with Kolliphor® P188, demonstrated a reduced droplet size of 136.48 ± 1.8 nm, a decreased PDI of 0.102 ± 0.00, and a zeta potential of −46.8 ± 2.5 mV, indicating improved size uniformity. Both formulations exhibited stability at the nanoscale (<200 nm) throughout accelerated and three-month stability evaluations. F6P2 showed the most favorable overall biological profile among the tested formulations, demonstrating pronounced antioxidant properties (DPPH IC_{50} = 22.65 µg/mL; ABTS IC_{50} = 10.42 µg/mL), along with 80.11 ± 0.04% inhibition of lipoxygenase and 76.9 ± 0.03% inhibition of tyrosinase at a dosage of 20 µg/mL.

Conclusion The developed NEGs loaded with *G. glabra* and *A. hippocastanum* demonstrated robust nanoscale stability together with notable antioxidant, anti-inflammatory, and anti-tyrosinase activities. The findings indicate that both biosurfactant-based and hybrid surfactant systems can be strategically tailored to balance colloidal stability and biological performance. Their potential as innovative dermocosmetic platforms for periorbital concerns is supported by their multifunctional relevance to pigmentation- and edema-associated pathways, warranting further in vivo evaluation.

Keywords *Glycyrrhiza glabra* · *Aesculus hippocastanum* · Herbal extracts · Nanoemulgel · Periorbital hyperpigmentation · Edema · Antioxidant · Anti-inflammatory · Anti-tyrosinase

✉ Ebru Altuntaş
ebru.altuntas@istanbul.edu.tr

Vildan Manav
drvildanmanav@gmail.com

Merve Yılmaz
merveyilmaz4@ogr.iu.edu.tr

Ayşe Esra Karadağ
aeguler@medipol.edu.tr

[1] Department of Pharmaceutical Technology, Faculty of Pharmacy, Istanbul University, Istanbul, Turkey

[2] Graduate School of Health Sciences, Istanbul University, Istanbul, Turkey

[3] University of Health Sciences, Istanbul Teaching and Research Hospital, Istanbul, Turkey

[4] Department of Pharmacognosy, School of Pharmacy, Istanbul Medipol University, Istanbul, Turkey

Published online: 14 May 2026

Introduction

Under-eye edema and periorbital hyperpigmentation (POH) are common aesthetic concerns that negatively affect patients' quality of life and result in a fatigued appearance [1]. These conditions have a complex etiology that includes vascular congestion, excessive melanin deposition, genetic predisposition, skin thinning, and lifestyle factors like stress and lack of sleep [2]. The periorbital area is one of the most delicate facial regions, where even minor changes can significantly affect appearance [3]. Currently, prescribed treatments may include the application of topical depigmenting agents (e.g., hydroquinone, kojic acid), chemical peeling, laser therapy, as well as injectable fillers and surgical interventions. Many such techniques have well-documented limitations, including skin irritation, rebound hyperpigmentation, and limited efficacy against underlying vascular or structural causes [4]. Conventional depigmenting topical formulations are often limited by poor aqueous solubility, chemical instability, and insufficient skin penetration of active substances [5, 6]. Hence, novel skin delivery systems are urgently needed to improve the stability and bioavailability of bioactive agents for periocular application [7].

Herbal extracts are increasingly used as safer alternatives for artificial depigmenting agents. Commonly referred to as licorice root, *Glycyrrhiza glabra* (*G. glabra*) is rich in glabridin, a flavonoid that has been shown to have potent anti-inflammatory and antioxidant effects, inhibit tyrosinase, and reduce the production of melanin. Therefore, this compound shows significant potential as a treatment for photoaging and hyperpigmentation [8, 9]. Similarly, *Aesculus hippocastanum (A. hippocastanum)*, or horse chestnut, contains escin, a saponin with well-established venotonic, anti-inflammatory, and antioxidant benefits. This compound has been demonstrated to enhance microcirculation and alleviate edema in conditions related to periorbital and venous insufficiency [10–12].

Nanoemulgel (NEG) formulations have recently gained prominence in cosmeceutical research because of their high drug-loading capacity, enhanced skin penetration, and superior physicochemical stability [13]. Their biphasic nature combines the benefits of gels and nanoemulsions (NEs), allowing bioactives to penetrate the skin more deeply while still being easily applied topically [13]. Notably, previous studies have shown that the incorporation of natural biosurfactants such as Quillaja saponin increases biological activity and emulsification efficiency, thus expanding the potential of NEG systems [14].

Recent studies indicate that NE-based technologies serve as effective vehicles for delivering depigmenting agents and improving their dermal efficacy; however, their application in POH has not yet been systematically investigated. Quercetin-loaded olive oil NEs demonstrate significant antioxidant activity (92%) and tyrosinase inhibition (56%), indicating their potential in modulating melanogenesis [15]. Similarly, azelaic acid-loaded NEs have demonstrated enhanced skin penetration and depigmenting efficacy, validating their application in hyperpigmentary skin disorders [16]. In vivo studies validate this approach, since NEs containing *Artocarpus incisus* extract significantly reduced UVB-induced hyperpigmentation in murine models [17]. Kojic monooleate-based NEs have been recognized as efficient vehicles for skin-lightening purposes, due to their ability to enhance the solubility and delivery of active compounds [18].

Despite these encouraging findings, current literature predominantly focuses on general hyperpigmentation and melasma, whereas studies specifically targeting the periorbital region are scarce. Recent comprehensive reviews on POH therapy notably fail to acknowledge NEs as either a novel or established therapeutic option, hence highlighting this gap in the literature [9, 19].

Given the need for topical systems that can improve dermal delivery while maintaining formulation stability and ease of application in the delicate periorbital region, NEG-based approaches emerge as a rational formulation strategy.

Accordingly, although interest in NE-based dermocosmetic systems and plant-derived depigmenting agents is increasing, no previous study has systematically integrated *G. glabra* and *A. hippocastanum* extracts into a NEG platform aimed at addressing both POH and edema at the same time. Furthermore, while natural surfactants like Quillaja saponin have been studied in food and pharmaceutical NEs, their comparative assessment against hybrid biosurfactant–synthetic systems in dermocosmetic NEGs is still limited. On this basis, this study explores a formulation design strategy by comparing saponin-based and hybrid surfactant systems, linking physicochemical stability with multifunctional biological performance. By integrating physicochemical stability assessment with antioxidant, anti-inflammatory, and anti-tyrosinase evaluations, this work provides new insights into the rational design of multifunctional NEG systems for delicate periorbital applications. Therefore, the novelty of this study lies in the integration of two plant extracts within a single NEG platform together with a systematic comparison of biosurfactant and hybrid surfactant systems, establishing a direct link between interfacial design and multifunctional dermocosmetic performance.

Materials and Methods

Materials

Quillaja saponaria saponins (Q-Naturale® 200 V, Ingredion GmbH, Germany) and Kolliphor® P 188 (Sigma-Aldrich, Germany) were used as surfactants, and Transcutol® HP (Gattefossé, France) was used as a co-surfactant. The oil phase contained caprylic/capric triglyceride (MCT; Croda, Türkiye) and Sensiva™ PA 30 (Ashland, Türkiye). DL-α-tocopherol acetate (Sigma-Aldrich, Germany) was added as an antioxidant. Xanthan gum (Vanzan® NF-C, Vanderbilt Minerals, USA) was used to formulate the gel. Reference standards of glabridin (Cayman Chemical, USA) and aescin (Sigma-Aldrich, Germany) were used for HPLC quantification. Distilled water (Merck Millipore, Germany) was used throughout the experiments. All the rest of the excipients were of analytical grade.

Distilled water was supplied by a PureLAB UV/UF Ionpure distillation system (USA). Filtration was performed using Whatman No. 1 filter papers (Cytiva, UK). Rotary evaporation was carried out using a Buchi Rotavapor R-100 (BÜCHI Labortechnik AG, Switzerland). Extracts were freeze-dried using a Christ Alpha 1–4 LSC lyophilizer (Martin Christ, Germany). Formulation steps were performed using a VCX 750 probe sonicator (Sonics & Materials Inc., USA) and a WiseStir HS-100D mechanical stirrer (DAIHAN Scientific Co. Ltd., South Korea). Centrifugation procedures employed a Nüve NF-series centrifuge (Nüve San. Malz. İm. ve Tic. A.Ş., Türkiye). Accelerated thermal stability assessments were performed using a WiseBath water bath (DAIHAN Scientific Co. Ltd., South Korea). Refrigerated storage was performed using an Indesit laboratory refrigerator (Italy). Accelerated and controlled stability studies were conducted inside a Nüve climate chamber (Nüve San. Malz. İm. ve Tic. A.Ş., Türkiye). Droplet size, polydispersity index (PDI), and zeta potential were measured using a Zetasizer Nano ZS (Malvern Instruments, UK). pH and electrical conductivity values were obtained using a Hanna Edge multiparameter meter (Hanna Instruments, USA). Viscosity measurements were performed with a Brookfield DV3T viscometer (AMETEK Brookfield, USA), while texture profile analysis was carried out using a CT3 Texture Analyzer (AMETEK Brookfield, USA). UV–Vis absorbance measurements were conducted using a Shimadzu UV-1800 spectrophotometer (Shimadzu, Japan). High-performance liquid chromatography (HPLC) analyses were performed using an Agilent 1100 system equipped with an ultraviolet–diode array detector (UV-DAD detector) (Agilent Technologies, USA).

Preparation of Standardized Plant Extracts

Plant Identification and Voucher Information

The fruits of *A. hippocastanum* were collected from mature trees located in the botanical garden area of Istanbul University. Botanical authentication was performed by Assoc. Prof. Dr. Ayşe Esra Karadağ, Department of Pharmacognosy, Faculty of Pharmacy, Istanbul Medipol University, based on macroscopic diagnostic characteristics consistent with the European Pharmacopoeia monograph. The roots of *G. glabra* were obtained from a local herbal market (Istanbul, Türkiye). The crude drug was identified according to its characteristic morphological features described in the European Pharmacopoeia. A laboratory voucher specimen representing both plant materials was prepared and deposited in the Pharmacognosy Department collection, Faculty of Pharmacy, Istanbul Medipol University, under the voucher code NEG-GG-AH-2025, for future reference.

Extraction

Powdered plant materials were accurately weighed and extracted with 80% methanol by continuous shaking for 24 h at room temperature. Following extraction, the suspensions were passed through Whatman No. 1 filter paper, and a rotary evaporator was used to concentrate the filtrates under reduced pressure. The concentrated extracts were stored at − 80 °C until further analysis. Finally, the extracts were lyophilized using a Christ Alpha 1–4 LSC lyophilizer (Martin Christ, Germany) for 48 h to obtain completely dried residues, which were subsequently used for analytical and biological experiments. This procedure follows previously reported methods for the preparation of standardized plant extracts [20, 21].

HPLC Analysis of Plant Extracts

The chemical profiles of *G. glabra* and *A. hippocastanum* extracts were determined using a HPLC system equipped with a UV-DAD. Chromatographic separation was carried out on a C18 reversed-phase analytical column (250 × 4.6 mm, 5 µm; Agilent Technologies, USA) under isocratic conditions, with specific mobile phases and detection wavelengths optimized for each marker compound. The phytochemical analysis was performed quantitatively using external calibration curves of the reference standards (glabridin and aescin). Linearity was confirmed within the tested concentration range (0.1–0.5 mg/mL), with correlation coefficients (R^2) greater than 0.99. Quantification of the

marker compounds was conducted to ensure batch-to-batch consistency and quality control of the raw plant materials prior to formulation development. All samples were filtered through a 0.45 µm membrane filter prior to injection. The quantitative determination of glabridin and aescin was performed using previously validated HPLC methods reported by Shanker et al. (2007) [20] and Durante et al. (2021) [21]. The chromatographic conditions were adopted without modification from these validated protocols. In accordance with ICH Q2(R1) guidelines [22], when a validated analytical method is implemented without alteration, full revalidation is not required. Linearity, precision, accuracy, and sensitivity parameters were therefore considered established based on the original validation studies.

Analysis of Glycyrrhiza glabra Extract The lyophilized *G. glabra* extract was dissolved in methanol at a concentration of 10 mg/mL and filtered through a membrane filter (0.45 µm) before being analyzed. The reference standard glabridin was dissolved in ethanol at 5 mg/mL and was then diluted with ethanol to obtain calibration concentrations of 0.1, 0.2, 0.3, 0.4 and 0.5 mg/mL. Chromatographic separation was performed under isocratic conditions using a mobile phase consisting of acetonitrile and 2% acetic acid in water (70:30, v/v) at a flow rate of 1.0 mL/min. The injection volume was 20 µL, and the column temperature was kept at 30 °C. Detection was carried out at 280 nm as described by Shanker et al. (2007) [20]. Peak identity was confirmed by retention time comparison with the reference standard, and quantification was performed using the external standard method.

Analysis of Aesculus Hippocastanum The lyophilized *A. hippocastanum* extract was dissolved in methanol (1 mg/mL) and filtered through a 0.45 µm filter, before being subjected to analysis. A standard aescin was dissolved in methanol at 5 mg/mL and diluted to obtain calibration levels of 0.1–0.5 mg/mL. Chromatographic separation was carried out using a mobile phase composed of acetonitrile and 0.1% phosphoric acid in water (40:60, v/v) under isocratic conditions, with a flow rate of 1.0 mL/min, injection volume of 20 µL, and a column temperature of 25 °C. Detection was performed at 210 nm, following the conditions reported by Durante et al. (2021) [21]. Peak identity was confirmed by retention time comparison with the reference standard, and quantification was performed using the external standard method.

Preparation of Nanoemulsions

A rational, stepwise optimization approach was employed during NE development. The formulation variables were adjusted systematically, including (i) the surfactant system (*Q. saponaria* saponins alone vs. saponin–Kolliphor® P188 combinations), (ii) surfactant-to-oil ratios, and (iii) sonication duration (5–10 min). These factors were chosen based on their recognized impact on droplet size, PDI, zeta potential, and physical stability.

Each formulation was assessed according to established quality criteria: droplet size < 200 nm, PDI < 0.30, absolute zeta potential > |30| mV, and stability under centrifugation and thermal stress. Formulations meeting these criteria advanced to biological tests.

The ultrasonic emulsification method was employed to create NEs with a consistent surfactant mixture (S-Mix) concentration of 15% w/w across all formulations. Research suggests that this technique yields kinetically stable dispersions with small droplet sizes suitable for skin delivery [23–26]. Two distinct S-Mix systems were examined:

System I: Q-Naturale® (12.5% w/w) + Transcutol® HP (2.5% w/w), based on the use of Quillaja saponins as natural biosurfactants with strong emulsification capacity and biocompatibility [27, 28].

System II: Q-Naturale® (10% w/w) + Kolliphor® P188 (2.5% w/w) + Transcutol® HP (2.5% w/w), following previous reports where mixed surfactant systems improved droplet size control and long-term stability [14, 29].

The oil phase comprised caprylic/capric triglyceride, Sensiva® PA 30, DL-α-tocopherol acetate, and Transcutol® HP, consistent with earlier studies where penetration enhancers and antioxidants were incorporated into the oil domain to improve dermal tolerability and protect essential oils from degradation [30–32]. Transcutol® HP was used as a co-surfactant in the NE system. Sensiva® PA 30 was incorporated as a preservative system to ensure microbiological stability. Propanediol served as a solvent and humectant, while tocopherol was included to enhance oxidative stability of the formulations.

The aqueous phase was composed of distilled water mixed with Q-Naturale® (and Kolliphor® P188 for System II) along with the specified plant extracts, following the standard procedure of dispersing hydrophilic actives or extracts in the external aqueous phase.

Formulations were prepared with oil phase concentrations of 5%, 7.5%, and 15% w/w, resulting in oil: S-Mix ratios of 1:3, 1:2, and 1:1, respectively. These specific ratios were selected because previous optimization research indicated that the proportion of oil to surfactant significantly influences the size, PDI, and stability of NEs [33, 34].

The oil and water phases were prepared separately and weighed exactly according to the design of the formulation. Then, the aqueous phase was carefully added to the oil phase and mixed by hand with a glass rod. This made a coarse pre-emulsion. A probe sonicator was used to further

process the coarse emulsion. It worked at 50% amplitude in a pulsed cycle (30 s on, 30 s off). Sonication lasted for 5–10 min, depending on the group of formulations. These sonication durations were selected based on previously published nanoemulsification studies indicating that ultrasonication for 5–10 min is sufficient to produce nano-sized droplets with low PDI, while prolonged sonication mainly increases temperature without further improving droplet size [25, 26, 35, 36]. To limit the increase in temperature and avoid the merging of droplets or the thermal breakdown of delicate components, the dispersion vessel was submerged in an ice bath during sonication [25]. Table 1 lists the formulations' composition and manufacturing specifications in detail.

Preparation of Nanoemulgels

To address the low viscosity and poor skin retention of NEs, specific NEs were incorporated into xanthan gum-based hydrogels to create NEGs. First, xanthan gum (1.5% w/w) was mixed with distilled water and stirred continuously at 400 rpm and 80 °C for 30 min. It was then cooled to room temperature. The hydrated gels were then mixed with the chosen NEs at a ratio of 1:1 (w/w) using magnetic stirring at 500 rpm for 10 min. The prepared NEGs were then left for 24 h to allow any air bubbles to escape and ensure uniformity of the system.

Characterization of Formulations

Droplet Size, Polydispersity Index (PDI), and Zeta Potential

Droplet size and PDI of NEs and NEGs were determined using dynamic light scattering (DLS) at 25 ± 0.1 °C with a 173° backscattering angle (non-invasive backscatter, NIBS) with a Zetasizer Nano ZS (Malvern Instruments, UK). Samples were diluted 100-fold with distilled water to minimize multiple scattering [37].

Zeta potential was measured using the same instrument by electrophoretic light scattering (ELS) at 25 °C, using folded capillary cells under automatic electric field settings. Droplet size, PDI, and zeta potential measurements were performed in six replicates, and results are expressed as mean ± SD.

pH and Electrical Conductivity

The pH values of the formulations were directly obtained with a calibrated digital pH meter, while electrical conductivity was examined utilizing a portable conductivity meter (Hanna Edge, USA) at 25 ± 2 °C. All measurements were conducted in triplicate [38].

Viscosity and Rheological Behavior

Viscosity was determined with a Brookfield cone and plate viscometer (spindle CP-40) at 25 ± 0.5 °C. Flow curves were obtained by plotting shear rate against viscosity to assess rheological behavior [39].

Accelerated Stability Testing

Physical stability was evaluated using centrifugation (3500 rpm, 30 min) and thermal stress assessments (40–80 °C, 5 °C increments, 30 min each) [40]. Furthermore, samples were preserved for three months at 5 ± 3 °C, 25 ± 2 °C with 60% relative humidity, and 40 ± 2 °C with 75% relative humidity. Periodic assessments encompassed droplet size, PDI, zeta potential, pH, viscosity, and conductivity.

Texture Profile Analysis (TPA)

A CT3 Texture Analyzer (Brookfield, UK) was utilized to determine the texture properties of NEGs, such as hardness, compressibility, adhesiveness, and cohesiveness [41]. A

Table 1 Composition of nanoemulsion-based formulations containing plant extracts

	Components	Composition of formulations (F1–F6)*					
	(% w/w)	F1	F2	F3	F4	F5	F6
Oil Phase	DL-alpha tocopherol acetate	0.2	0.2	0.2	0.2	0.2	0.2
	Caprylic/capric triglyceride	2.8	5.3	12.8	2.8	5.3	12.8
	Sensiva® PA 30	2	2	2	2	2	2
	Transcutol® HP	2.5	2.5	2.5	2.5	2.5	2.5
Hydrophilic Phase	*G. glabra* extract	2	2	2	2	2	2
	A. hippocastanum extract	2	2	2	2	2	2
	Kolliphor® P 188	-	-	-	2.5	2.5	2.5
	Q-Naturale® 200 V	12.5	12.5	12.5	10	10	10
	Distilled Water (d.w.)	qs to 100	qs to 100	qs to 100	qs to 100	qs to 100	qs to 100
Process	**Process 1 (P1)**: 5 min ultrasound emulsification **Process 2 (P2)**: 10 min ultrasound emulsification						

* All formulations (F1–F6) were prepared using two different processes: P1 = 5 min ultrasound emulsification, P2 = 10 min ultrasound emulsification

12.7 cm analytical probe was applied twice on each sample at a specified depth and velocity, allowing for recovery periods between compressions.

Antioxidant Activity

DPPH Radical Scavenging Assay

The antioxidant activity of the formulations was tested by using the 2,2-diphenyl-1-picrylhydrazyl (DPPH) radical scavenging technique [42]. In summary, 0.1 mL of the test sample (0.16–2.5 mg/mL) or the standard antioxidant quercetin (0.01–0.31 mg/mL) was combined with 3.9 mL of DPPH solution in methanol (6×10^{-5} M). The mixture was vortexed and incubated in the absence of light for 30 min at ambient temperature. The reduction in absorbance was quantified at 517 nm with a UV-Vis spectrophotometer, with methanol serving as the blank. Quercetin functioned as the positive control, whereas methanol acted as the negative control. Each test was conducted in triplicate, and the average data were utilized to determine the percentage inhibition of the DPPH radical according to Eq. 1.

$$\%Inhibition = \frac{A_{control} - A_{sample}}{A_{control}} \times 100 \quad (1)$$

ABTS Radical Cation Decolorization Assay

The overall antioxidant capacity of the samples was further assessed utilizing the 2,2′-azino-bis(3-ethylbenzothiazoline-6-sulfonic acid) (ABTS) test as previously stated [43]. The $ABTS^+$ radical cation was produced by combining a 7 mM ABTS solution with 2.45 mM potassium persulfate and permitting the combination to incubate in the dark at room temperature for 12 to 16 h prior to use. The $ABTS^+$ solution was diluted with ethanol (pH 7.4) to achieve an absorbance of 0.700 ± 0.02 at 734 nm.

The test samples were suitably diluted and combined with $ABTS^+$ solution to achieve a final volume of 1 mL for the experiment. Following a 6-minute incubation at ambient temperature, the absorbance was measured at 734 nm. Trolox functioned as the positive control, whereas ethanol acted as the negative control. The % inhibition of $ABTS^+$ was determined using the previously mentioned formula.

Anti-inflammatory Activity: Lipoxygenase (LOX) Inhibition Assay

Using the spectrophotometric method developed by Baylac and Racine (2003) [44], the formulations' inhibitory effect on the activity of the lipoxygenase (LOX) enzyme was used to evaluate their anti-inflammatory properties. 20 µL of the lipoxygenase enzyme solution, 40 µL of the test sample solution, and 1.97 mL of potassium phosphate buffer (100 mM, pH 9.0) made up the reaction mixture. 50 µL of linoleic acid solution was added as a substrate after the mixture had been incubated for 10 min at 25 °C. Using a UV-Vis spectrophotometer, the absorbance change was observed at 243 nm for 20 min. Methanol was employed as the negative control, and nordihydroguaiaretic acid (NDGA) as the positive control. Every experiment was run in triplicate.

Tyrosinase Inhibition Assay

The ability of the formulations to inhibit tyrosinase was determined following the methods of Hearing and Jiménez (1987) with minor alterations [45]. In summary, mushroom tyrosinase (30 U, 28 nM) was diluted with sodium phosphate buffer (50 mM, pH 6.8). The enzyme solution was pre-incubated with test compounds for 10 min at room temperature. The enzymatic reaction was initiated with the addition of 0.5 mM L-DOPA as the substrate. The rise in the absorbance at 475 nm and 37 °C due to the formation of dopachrome was monitored. The positive control was established with Kojic acid. The percentage of inhibition of tyrosinase activity was determined following Eq. 2.

$$\%Inhibition = \frac{A_{control} - A_{sample}}{A_{control}} \times 100 \quad (2)$$

where $A_{control}$ is the absorbance of the reaction mixture without sample and A_{sample} is the absorbance in the presence of the test formulation.

Statistical Analysis

All measurements for droplet size, PDI, and zeta potential were performed in six replicates ($n=6$) for each stability condition (Day 1, centrifugation, and thermal stress). For three-month storage stability evaluation (5 °C, 25 °C, and 40 °C), droplet size, PDI, and zeta potential measurements were also performed in six replicates ($n=6$) at each time point (Day 1, Month 1, Month 2, and Month 3). pH, conductivity, and viscosity measurements were conducted in triplicate ($n=3$).

Pairwise statistical comparisons between T0 (Day 1) and the post-stress conditions were conducted using a two-tailed Welch's t-test, which does not assume equal variances between groups. For long-term storage evaluation, pairwise comparisons were conducted between Day 1 and Month 3 values at each storage temperature using Welch's two-tailed independent t-test. In addition, selected inter-formulation comparisons at T0 were performed between representative saponin-based and hybrid systems using Welch's two-tailed

independent t-test to evaluate baseline differences in physicochemical parameters.

Statistical significance was defined as $p<0.05$. Welch's t-test was selected due to its robustness in handling independent measurements and potential variance heterogeneity across time points. Detailed numerical results and p-values for stability comparisons are provided in Supplementary File S1, while the main manuscript reports only the summary interpretation of statistical outcomes. All statistical analyses were performed using Python (SciPy statistical package, Python Software Foundation).

Results and Discussion

Phytochemical Analysis of Plant Extracts

HPLC analyses conducted for the standardization of herbal extracts validated the existence of α- and β-escin in *A. hippocastanum extract*, and glabridin in *G. glabra extract*. Escin A (tR ≈ 11.6–11.7 min) and escin B (tR ≈ 13.2–13.3 min) were observed as distinct peaks in the obtained chromatograms (Fig. 1), and these results were found to be consistent with the characteristic retention times of saponins obtained from *A. hippocastanum* seeds in the literature [46, 47]. Similarly, when compared with the standard substance, the peak observed at tR ≈ 6.0 min in *G. glabra* extract confirmed the presence of glabridin (Fig. 2). This finding is in line with previous studies reporting that glabridin can be reliably separated from methanolic extracts by RP-HPLC method [20]. Consequently, the pharmacological effects of these extracts can be considered more consistent and reproducible through the quantification of escin and glabridin as marker compounds. Additionally, the distinct but complementary biological activities of these compounds (glabridin's antioxidant and anti-melanogenic effects, and escin's anti-edematous/venotonic properties) suggest a potential complementary dermocosmetic effect when combined. These findings support the rationale for the combination-based formulation strategy.

Formulation Design Strategy and Optimization Parameters

The under-eye area is one of the most sensitive and aesthetically critical zones of the face. Cosmetic concerns such as hyperpigmentation and edema are associated with aesthetic and morphological changes in the periorbital region. As personal aesthetics gain more prominence, the demand for safe, effective, and multifunctional dermocosmetic solutions is

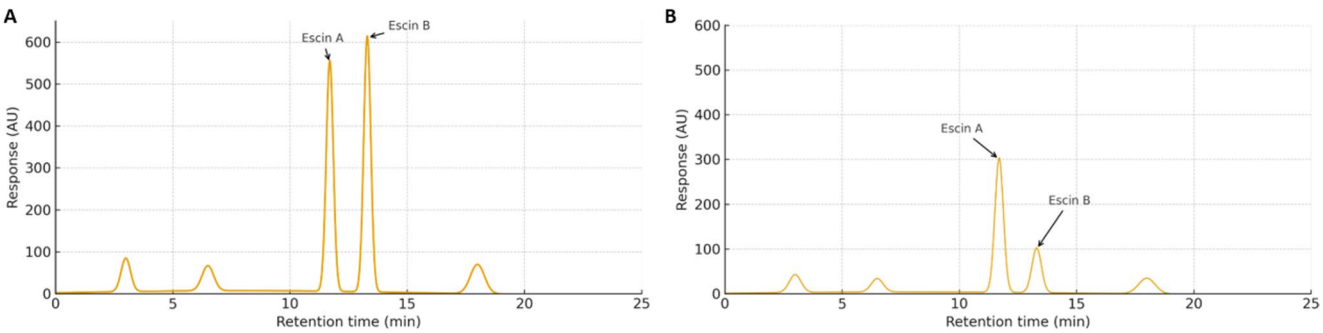


Fig. 1 Representative HPLC chromatograms. Escin standard showing two major saponin peaks (Escin A and Escin B) (**A**) and *A. hippocastanum* extract chromatogram displaying corresponding saponin peaks (**B**)

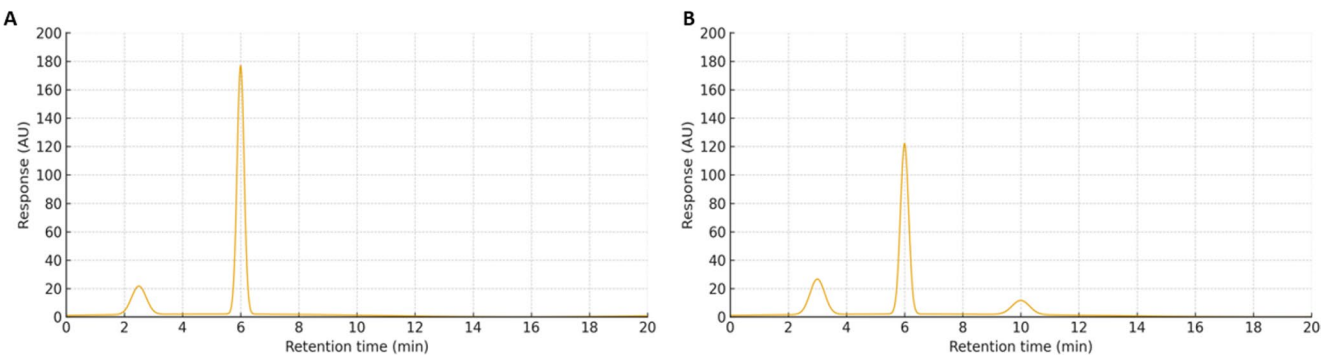


Fig. 2 Representative HPLC chromatograms. Glabridin standard showing the characteristic peak at tR ≈ 6.0 min (**A**) and *G. glabra* extract chromatogram displaying the corresponding glabridin peak (**B**)

rapidly increasing [3, 48]. The current study was designed using the phytochemical-based formulation strategy which involves using extracts of *G. glabra* (licorice) and *A. hippocastanum* (horse chestnut). Licorice root has bioactive flavonoids, namely glabridin and liquiritin, with depigmenting, antioxidant, and anti-inflammatory effects, rendering it an interesting candidate treatment for the management of POH [49, 50]. Horse chestnut extract containing escin saponins shows venotonic and anti-edematous activities which are associated with an increase in microcirculatory tone and a decrease in capillary permeability. This effect supports its potential role in the treatment of eyelid puffiness and periocular edema [10]. The combined use of these extracts may provide complementary biological effects in the management of POH and eyelid edema.

Recent studies focus on combination therapies using plant-derived actives and employing novel topical delivery systems, which may offer complementary or enhanced biological effects along with improved skin compatibility [51]. In this study, Q-Naturale® 200 was used either alone or mixed with Kolliphor® P188 to represent two different stabilization strategies. Hybrid biosurfactant–synthetic systems are gaining attention as they provide a spectrum, as well as a combination, of advantageous interfacial packaging, low toxicity, and improved physicochemical stability in the comparison with monosurfactant systems [52, 53].

The selection of additional formulation components was guided by their functional contributions to NE stability and dermal compatibility. Q-Naturale® was employed as the primary biosurfactant due to its strong emulsifying capacity and ability to provide electrostatic stabilization [27]. Kolliphor® P188 was incorporated to enhance steric stabilization and improve droplet size distribution in hybrid surfactant systems, consistent with previous reports demonstrating the role of nonionic surfactants in reducing droplet aggregation and improving NE stability [14, 29]. Transcutol® HP was employed as a cosurfactant in the NE system. Due to its amphiphilic structure and low molecular weight, Transcutol® HP may reduce interfacial tension and enhance surfactant packing at the oil–water interface, thereby facilitating the formation of smaller droplet sizes and improving kinetic stability of NEs. Moreover, it has a well-established history of use in topical pharmaceutical and dermocosmetic formulations with documented low irritancy potential, making it suitable for sensitive-skin applications [54, 55].

Sensiva® PA 30 (Propanediol (and) Phenethyl Alcohol (and) Undecyl Alcohol (and) Tocopherol) was incorporated as a multifunctional antimicrobial/preservative blend to support microbiological stability of the dermocosmetic formulations. Alternative preservative approaches based on aromatic alcohols, such as phenethyl alcohol, have been increasingly explored in the cosmetic preservation literature as multifunctional antimicrobial systems [56]. Propanediol contributes as a solvent/humectant and has also been evaluated in the context of preservative effectiveness and skin compatibility in cosmetic applications [57, 58]. Tocopherol was included to support oxidative stability, consistent with reports demonstrating improved oxidative stability of O/W emulsions upon tocopherol incorporation [59]. Caprylic/capric triglycerides were selected as the oil phase due to their favorable dermal compatibility and widespread use as non-irritant emollients, as well as their contribution to the physicochemical stability of nanoemulsion systems [60].

Effect of Oil Phase Ratio and Sonication Time on Nanoemulsion Characteristics

Oil phase concentrations of 5%, 7.5%, and 15% w/w were used to create the NEs; these corresponded to oil: S-Mix ratios of 1:3, 1:2, and 1:1, respectively. To assess the impact of sonication time, two ultrasonication protocols—P1 (5 min) and P2 (10 min)—were used. Consistent with earlier research, a longer ultrasonication duration typically results in narrower size distributions and smaller droplet sizes because it increases energy input and enhances cavitation-induced droplet disruption [24]. Furthermore, a recent comparative study verified that, in contrast to shorter treatments (such as 5 min) or alternative technologies, ultrasonication at 50% amplitude for 10 min resulted in noticeably smaller droplets and lower PDI values [61]. This research showed that ultrasonication at 50% amplitude for 10 min resulted in reduced droplet size and lower PDI values compared to 5 min treatments, confirming the benefits of extended sonication time.

As reported in previous studies, the concentration of the oil phase along with the type of oil, plays a critical role as the volume affects the size of the droplet, uniformity of distribution, the efficiency of packing at the interface, and the arrangement of emulsions over the long term stability of emulsions [62]. Changes in oil volume can alter droplet dynamics and, consequently, the physicochemical behavior of the system. Table 2 presents the droplet size, PDI, and zeta potential measurements of the formulations on Day 1 and following accelerated stability assessments, including centrifugation and thermal stress. In our study, the 15% oil formulation (F3) had the best colloidal properties for the Quillaja saponins-stabilized group (F1–F3), with the smallest droplet size (145.1 nm), lowest PDI (0.203), and the most negative zeta potential (–69.2 mV). In contrast, the 7.5% oil formulation (F2) displayed the lowest desirability values (202.8 nm, PDI 0.278, − 64.2 mV), while the 5% oil formulation (F1) produced a larger droplet size (174.0 nm, PDI

Table 2 Droplet size (nm), PDI, and zeta potential (mV) of nanoemulsions at day 1 and after accelerated stability tests (centrifugation and thermal stress) (mean ± SD, $n = 6$)

Code	Mean droplet size (nm)			PDI			Zeta potential (mV)		
	T0	ACT	ATT	T0	ACT	ATT	T0	ACT	ATT
F1P1	216.0 ± 4.3	210.4 ± 4.7	233.2 ± 1.4	0.345 ± 0.00	0.325 ± 0.03	0.367 ± 0.01	-64.0 ± 2.5	-64.6 ± 2.4	-62.3 ± 1.9
F1P2	174.0 ± 7.2	194.9 ± 5.4	187.8 ± 0.8	0.206 ± 0.00	0.269 ± 0.03	0.233 ± 0.01	-67.5 ± 3.0	-60.6 ± 0.1	-59.5 ± 1.6
F2P1	263.3 ± 16.1	282.7 ± 25.2	264.3 ± 3.9	0.388 ± 0.04	0.321 ± 0.04	0.304 ± 0.06	-66.8 ± 1.0	-59.3 ± 1.4	-60.2 ± 2.6
F2P2	202.8 ± 10.7	238.8 ± 8.2	241.0 ± 9.6	0.278 ± 0.00	0.337 ± 0.06	0.288 ± 0.03	-64.2 ± 1.2	-61.2 ± 2.6	-58.5 ± 1.5
F3P1	183.0 ± 1.0	188.8 ± 2.5	198.1 ± 3.6	0.206 ± 0.02	0.188 ± 0.02	0.167 ± 0.01	-65.0 ± 1.9	-62.8 ± 1.4	-62.7 ± 3.0
F3P2	145.1 ± 3.4	147.8 ± 5.9	157.3 ± 4.5	0.203 ± 0.01	0.155 ± 0.03	0.121 ± 0.03	-69.2 ± 1.1	-62.0 ± 4.8	-55.0 ± 1.7
F4P1	148.4 ± 4.0	154.3 ± 2.7	229.8 ± 2.6	0.136 ± 0.03	0.110 ± 0.03	0.131 ± 0.01	-46.1 ± 3.1	-46.2 ± 2.8	-42.5 ± 0.5
F4P2	177.7 ± 2.4	176.9 ± 1.6	241.7 ± 6.3	0.179 ± 0.02	0.121 ± 0.01	0.118 ± 0.05	-42.0 ± 3.4	-44.0 ± 1.8	-45.2 ± 0.6
F5P1	145.9 ± 3.2	152.1 ± 2.0	231.8 ± 3.4	0.144 ± 0.02	0.118 ± 0.04	0.069 ± 0.02	-39.0 ± 0.6	-42.2 ± 0.1	-41.7 ± 3.5
F5P2	135.6 ± 0.7	141.3 ± 0.2	213.3 ± 3.0	0.123 ± 0.02	0.090 ± 0.00	0.063 ± 0.01	-43.6 ± 1.7	-41.7 ± 0.8	-39.8 ± 1.3
F6P1	144.8 ± 2.1	151.9 ± 2.2	244.5 ± 6.8	0.117 ± 0.02	0.106 ± 0.02	0.078 ± 0.00	-45.9 ± 1.0	-43.0 ± 1.0	-46.1 ± 2.1
F6P2	137.6 ± 1.5	143.2 ± 3.5	232.6 ± 3.9	0.098 ± 0.02	0.080 ± 0.03	0.088 ± 0.02	-38.7 ± 2.4	-41.2 ± 1.0	-45.4 ± 1.4

*T0: before the accelerated stability tests; *ACT: after centrifuge test; *ATT: after thermal test

0.206, − 67.5 mV). Various elements may account for this result. To begin with, a higher oil concentration decreases the surfactant-to-oil interface ratio, leading to fewer droplets that are more effectively stabilized. The interfacial film created by Quillaja saponins is notably strong due to their amphiphilic glycoside structure, which provides both electrostatic repulsion and steric hindrance [63]. Thus, at 15% oil phase, the saponins probably reached optimal packing at the droplet interface and formed uniform nanodroplets with less polydispersity. Also, the oil phase composition itself improved stability. Caprylic/capric triglycerides and DL-α-tocopherol acetate are highly lipophilic and only sparingly soluble in water. This decreases the driving force for Ostwald ripening by inhibiting molecular diffusion between droplets [64]. Therefore, the 15% oil formulation not only resulted in smaller droplet sizes, but more narrow size distribution, which was maintained over time. Finally, higher oil fractions increase the effective viscosity of the dispersed phase. This decreases droplet movement and collision frequency; hence, coalescence is less likely [65]. These compositional and interfacial factors may account for the comparatively favorable physicochemical profile observed for F3 among the tested variants.

All three formulations also produced nanoscale droplets with low PDI values in the group that contained Kolliphor® P188 and Quillaja saponins (F4–F6) (Table 2). While F4 (5% oil) displayed somewhat larger droplets (177.7 nm, PDI 0.179, −42.0 mV), F5 (7.5% oil) and F6 (15% oil) performed similarly, with droplet sizes of 135.6 nm (PDI 0.123, −43.6 mV) and 137.6 nm (PDI 0.098, −38.7 mV), respectively. Despite having negligible differences in droplet size and PDI, F5 and F6 both performed noticeably better than F4, indicating that higher oil fractions once more enabled enhanced emulsification efficiency.

Comparative Evaluation of Saponin-Based and Hybrid Nanoemulsions

In comparing the two groups, the saponin-only formulation F3 exhibited a more negative zeta potential (–69.2 mV) than the saponin + Kolliphor systems (–38.7 to − 43.6 mV). This stronger interfacial charge is probably due to the acidic glycosidic moieties of Quillaja saponins, which provide substantial electrostatic stabilization [66]. However, the addition of Kolliphor® P188 seemed to synergistically work with saponins to reduce droplet size and PDI, particularly in F5 and F6, despite lower absolute surface charge. This indicates a compromise: systems with only saponin provide stronger electrostatic stabilization (higher zeta potential) and hybrid systems attain finer droplet size distributions (lower PDI) due to better interfacial packing. In terms of zeta potential and colloidal repulsion, F3 appeared to be the most electrostatically stable formulation overall, while F5 and F6 showed the smallest and most consistent droplet sizes of all the formulations. These complementary results demonstrate the potential benefit of combining synthetic and biosurfactants, namely lowering the synthetic load while preserving or even enhancing physicochemical stability. To further substantiate these compositional differences, a direct statistical comparison between the representative saponin-only (F3P2) and hybrid (F6P2) NEs at T0 was performed using Welch's two-tailed independent t-test ($n = 6$). Significant differences were observed in droplet size ($p = 0.0019$), PDI ($p < 0.001$), and zeta potential ($p < 0.001$). F6P2 exhibited significantly smaller droplet size and lower PDI, indicating improved homogeneity, whereas F3P2 demonstrated a significantly more negative zeta potential, reflecting stronger electrostatic stabilization. Importantly, despite these statistical differences, both formulations remained within

acceptable nanoscale and stability ranges (< 200 nm; |zeta potential| > 30 mV), confirming that the observed variations arise from surfactant composition rather than instability.

Recent findings indicate that nanoformulations with a negative surface charge may improve skin adherence and drug retention. Abruzzo et al. demonstrated that microemulsions loaded with azithromycin and possessing a negative zeta potential (ranging from − 22.32 to − 27.78 mV) achieved significantly greater skin accumulation (59.58 ± 3.49%) in ex vivo full-thickness porcine skin after 24 h, compared to neutral or positively charged counterparts (22.04 ± 3.99%) ($p < 0.05$) [67]. The researchers attributed the enhanced skin deposition to the natural negative charge of skin lipids, which facilitates favorable interfacial alignment and promotes reservoir-like retention of anionic colloidal systems within the stratum corneum and upper dermal layers. In the present study, the highly negative zeta potential values of the current NE formulations (approximately − 40 to − 70 mV) are anticipated to enhance colloidal stability and strengthen interfacial interactions with the periocular skin surface. In addition to the interfacial effects associated with the anionic surface charge, the presence of Transcutol® HP may further influence dermal delivery behavior. Transcutol® is widely recognized as a penetration-modulating excipient in topical formulations, primarily due to its ability to enhance solubilization of lipophilic actives and promote their partitioning into the stratum corneum. Its amphiphilic nature facilitates diffusion within the intercellular lipid domains without causing pronounced lipid disruption. Therefore, the combined effect of highly negative zeta potential and Transcutol-mediated penetration enhancement may contribute to enhanced localized dermal deposition of glabridin and escin [54].

Accelerated Stability Behavior of Nanoemulsions

After undergoing stress tests, the saponin-based and hybrid systems (saponin + Kolliphor® P188) generally displayed only minor changes in their physicochemical characteristics, staying within the acceptable stability limits (PDI < 0.3; zeta potential < − 30 mV). This implies that even under accelerated conditions, the NEs' colloidal stability was preserved. Statistical analysis (two-tailed Welch's t-test, $n = 6$), with full datasets and p-values provided in the Supplementary Material, indicated that certain stress-induced changes were statistically significant ($p < 0.05$). However, the magnitude of these changes remained within predefined physicochemical acceptance criteria (PDI < 0.3; zeta potential < − 30 mV) and did not affect the overall nano-scale integrity or homogeneity of the systems.

Among the formulations containing only saponin, F3P2 exhibited the most robust and statistically validated stability profile. After undergoing centrifugation and thermal stress, the mean droplet size showed only slight increases from 145 nm on Day 1 to 147 nm and 157 nm, respectively. Although the size increase following thermal stress was statistically significant, it was minor in extent ($p < 0.05$). Importantly, the PDI values significantly decreased under stress conditions (0.203 → 0.155 → 0.121; $p < 0.05$), suggesting a statistically significant enhancement in size distribution uniformity rather than destabilization. Additionally, the zeta potential of F3P2 remained highly negative throughout the stress tests (− 69.2 to − 55.0 mV). Despite statistical analysis showing a notable change in zeta potential values following stress exposure ($p < 0.05$), the magnitude of the surface charge consistently stayed well below − 30 mV, signifying maintained electrostatic stabilization. These results further corroborate the robust interfacial stabilizing ability of Quillaja saponins, as documented in earlier research [14, 63].

Hybrid NEs incorporating Kolliphor® P188 were found to have smaller initial droplet sizes compared to those with only saponin, as evidenced by the 137 nm size in F6P2. This indicates the size-reducing capability of the mixed surfactant system. Even though centrifugation and thermal stress led to a statistically significant increase in droplet size for F6P2 (137 → 143 → 232 nm; $p < 0.05$), the formulation continued to exhibit nano-scale dimensions (< 250 nm) and maintained satisfactory colloidal stability. Significantly, hybrid systems consistently recorded the lowest PDI values across all formulations, with F5P2 showing a marked reduction in PDI after stress (0.123 → 0.090 → 0.063; $p < 0.05$), suggesting that the synergistic interactions between saponins and Kolliphor® P188 resulted in a more compact and uniform interfacial film. Although the zeta potential values for hybrid systems (− 38 to − 46 mV) were lower than those for saponin-only formulations, statistical analysis confirmed that these values were still within the necessary range for electrostatic stabilization, and no stress condition caused a critical loss of surface charge.

Influence of Gel Incorporation on Colloidal Properties (NE vs. NEG Comparison)

The physicochemical parameters of NEGs (F1–F6) at Day 1 and after accelerated stability tests (centrifugation and thermal stress) are presented in Table 3. The comparison of initial physicochemical parameters (Day 1) between NEs and NEGs provides valuable insights into the effect of incorporating NEs into a hydrogel matrix. In comparison to their corresponding NEs, NEGs typically exhibited satisfactory PDI values and droplet sizes that were either lower or equivalent. This indicates that droplet mobility was constrained and kinetic stability was augmented by the gel matrix. For example, F1P1 decreased from 216 nm (NE) to

Table 3 Droplet size (nm), PDI, and zeta potential (mV) of nanoemulgels at day 1 and after accelerated stability tests (centrifugation and thermal stress) (mean ± SD, $n = 6$)

Code	Mean droplet size (nm)			PDI			Zeta potential (mV)		
	T0	ACT	ATT	T0	ACT	ATT	T0	ACT	ATT
F1P1	122.4 ± 4.2	190.6 ± 6.8	237.4 ± 3.7	0.199 ± 0.01	0.345 ± 0.00	0.392 ± 0.04	-49.2 ± 2.9	-64.6 ± 1.9	-59.9 ± 2.2
F1P2	185.6 ± 7.3	188.0 ± 9.8	197.8 ± 13.2	0.343 ± 0.01	0.343 ± 0.04	0.320 ± 0.05	-54.5 ± 1.2	-70.4 ± 5.1	-62.0 ± 3.1
F2P1	190.3 ± 4.9	196.6 ± 15.7	239.0 ± 15.0	0.389 ± 0.01	0.355 ± 0.05	0.432 ± 0.02	-58.2 ± 2.0	-59.6 ± 5.4	-62.4 ± 1.8
F2P2	220.4 ± 11.0	203.0 ± 5.3	216.0 ± 6.6	0.371 ± 0.01	0.292 ± 0.02	0.279 ± 0.01	-64.1 ± 3.1	-70.3 ± 2.5	-61.6 ± 4.9
F3P1	192.1 ± 2.4	197.0 ± 4.7	200.6 ± 1.3	0.220 ± 0.01	0.245 ± 0.01	0.243 ± 0.02	-65.7 ± 2.3	-76.9 ± 3.6	-64.6 ± 0.7
F3P2	142.7 ± 1.9	147.9 ± 2.4	162.5 ± 2.6	0.184 ± 0.01	0.238 ± 0.02	0.226 ± 0.00	-59.0 ± 3.3	-60.3 ± 1.5	-48.5 ± 4.5
F4P1	155.0 ± 3.1	170.0 ± 3.5	170.0 ± 5.4	0.250 ± 0.01	0.229 ± 0.02	0.149 ± 0.01	-46.4 ± 3.3	-54.6 ± 2.1	-46.5 ± 1.1
F4P2	138.1 ± 1.7	142.0 ± 6.1	133.6 ± 0.9	0.260 ± 0.02	0.221 ± 0.01	0.143 ± 0.02	-50.3 ± 3.9	-50.4 ± 2.5	-50.4 ± 1.6
F5P1	152.8 ± 1.4	156.4 ± 3.5	192.0 ± 3.9	0.235 ± 0.02	0.245 ± 0.02	0.192 ± 0.02	-50.9 ± 4.2	-52.0 ± 2.7	-51.9 ± 2.3
F5P2	139.8 ± 3.4	158.4 ± 0.8	218.4 ± 8.4	0.263 ± 0.02	0.217 ± 0.02	0.310 ± 0.04	-49.1 ± 1.7	-52.7 ± 5.6	-52.1 ± 3.0
F6P1	146.6 ± 0.9	152.8 ± 1.6	200.4 ± 3.1	0.123 ± 0.01	0.222 ± 0.02	0.189 ± 0.01	-46.2 ± 3.1	-60.0 ± 1.7	-59.2 ± 2.8
F6P2	136.5 ± 1.8	135.0 ± 2.6	184.8 ± 3.8	0.102 ± 0.00	0.197 ± 0.01	0.156 ± 0.01	-46.8 ± 2.5	-56.5 ± 10.7	-48.1 ± 1.7

*T0: before the accelerated stability tests; *ACT: after centrifuge test; *ATT: after thermal test

122 nm (NEG), although F3P2 remained relatively constant at around 145 nm in NE compared to 142 nm in NEG. The majority of NEGs exhibited values below 0.3, signifying a rather uniform size distribution; nevertheless, the impact on PDI varied among the formulations. In all systems, the zeta potential values were markedly negative (≤ -45 mV), indicating robust electrostatic stabilization independent of the gel network. In line with the patterns seen in the related NEs, a statistical analysis comparing F3P2 and F6P2 NEGs on Day 1 (using Welch's t-test, $n = 6$) revealed significant differences in droplet size, PDI, and zeta potential ($p < 0.001$). Importantly, integrating these into the gel matrix did not remove these compositional differences. The hybrid system (F6P2) maintained a notably smaller droplet size and lower PDI, suggesting that the interfacial packing efficiency within the hydrogel network was preserved. On the other hand, F3P2 exhibited a significantly more negative surface charge, indicating continued electrostatic stabilization. These results illustrate that while gel incorporation affects kinetic behavior, it does not change the systems' inherent surfactant-dependent stabilization characteristics. Generally, the introduction of a steric barrier by inclusion into a gel phase aligns with previous research indicating that gelling agents can enhance colloidal stability and reduce droplet coalescence [68].

Accelerated Stability of Nanoemulgels

The NEG formulations exhibited negligible alterations from Day 1 during accelerated stability testing, reliably preserving nanoscale droplet sizes below 250 nm across all formulations. Although certain formulations demonstrated statistically significant differences in mean droplet size post-centrifugation and thermal stress (two-tailed Welch's t-test, $n = 6$, $p < 0.05$; detailed values in Supplementary Table S2), these discrepancies were confined to an acceptable nanometric range and did not indicate physical destabilization. In certain instances, slight increases in size were noted (e.g., F1P1: 122 nm → 191 nm post-centrifugation and 237 nm post-thermal stress), whereas other formulations showed minimal or no change. Notably, PDI values generally stayed below 0.30 after both stress conditions, and although some formulations experienced statistically significant PDI shifts ($p < 0.05$), these did not affect droplet size uniformity. Zeta potential values became slightly more or less negative depending on the formulation and stress condition, with several changes reaching statistical significance ($p < 0.05$). Nonetheless, all NEG systems consistently maintained zeta potential values below −40 mV, a range deemed adequate for electrostatic stabilization. No creaming, sedimentation, or phase separation was observed in any formulation, confirming that statistically detectable physicochemical changes did not lead to macroscopic instability. Overall, statistical analysis confirmed that incorporating a gel matrix did not compromise NE stability and, in some cases, enhanced droplet size uniformity. Although not all parameters improved uniformly when transitioning from NEs to NEGs, the NEG systems successfully endured centrifugal and thermal stress while preserving nanoscale characteristics. These results demonstrate that NEGs effectively combine the solubilization capacity of NEs with the enhanced kinetic stability provided by a gel network, supporting their suitability as robust and reliable topical delivery systems.

Short-Term Stability Assessment of Selected Nanoemulgels

Due to their superior initial and stress test performance, NEGs F4P1, F4P2, F5P1, F5P2, F6P1, and F6P2 (saponin–Kolliphor® P188 hybrids) and F3P1 and F3P2 (saponin-only)

were selected for three-month physicochemical stability testing. These systems demonstrated homogenous and stable dispersions on Day 1 with low PDI values (≤0.3), strongly negative zeta potentials, and nanoscale droplet sizes (<200 nm in most cases). PDI values mostly stayed below 0.3 following centrifugation and thermal stress, droplet size changes were negligible, and no macroscopic instability (creaming, sedimentation, phase separation) was seen. Particularly, F3P2 among the saponin-only group and F5P2 and F6P2 among the hybrid systems showed outstanding homogeneity, supporting their robustness. Overall, these formulations demonstrated the most promising stability profiles, combining electrostatic stabilization from saponins with steric contributions from Kolliphor where applicable, and were therefore advanced to short-term stability studies.

To guarantee the effectiveness and user compliance of topical applications, it is essential to assess the storage stability of NEG formulations under defined conditions. According to the study, the selected formulations remained stable under a range of storage conditions, including cold (5 °C), accelerated (40 °C, 75% RH), and room temperature (25 °C, 65% RH), for up to three months without experiencing any physical deterioration.

Organoleptic examinations (color, odor, appearance, fluidity, creaming, and phase separation) confirmed that the formulations retained their initial properties throughout the storage period. In particular, the preparation of NEs using a saponin-derived biosurfactant contributed to the protection of the system through both electrostatic and steric stabilization mechanisms, and also explained the stability of the milky brown characteristic appearance. This finding is consistent with reports in the literature that saponins reduce droplet coalescence by providing strong packing and charge distribution in interfacial films [69, 70].

Regarding droplet size, most formulations exhibited minor differences in droplet size and stability under various storage conditions. As evidenced by the droplet size remaining largely consistent, low temperatures inhibit Ostwald ripening and droplet coalescence. Statistical comparison between Day 1 and Month 3 (Welch's two-tailed t-test, $n = 6$) showed no significant differences in droplet size at 5 °C and 25 °C for either F3P2 or F6P2 ($p > 0.05$). At 40 °C, statistically significant increases were observed ($p < 0.05$); however, the droplet sizes remained within the nanometric range and did not indicate physical destabilization. For instance, over a three-month span, F3P2 maintained a droplet size between approximately 135–140 nm, while F6P2 ranged from about 145–150 nm, indicating high stability at low temperatures. Although slight variations were noted at room temperature, the values remained under 200 nm, which is considered appropriate for topical use. As seen in previous studies, a slight to moderate increase in droplet size at 40 °C has been recorded with certain formulations [71, 72].

PDI values remained below 0.3 under all storage conditions. Statistical analysis confirmed that PDI values at 5 °C and 25 °C did not differ significantly from initial measurements ($p > 0.05$). Although minor variations reached statistical significance at 40 °C ($p < 0.05$), all PDI values remained below 0.3, indicating preserved droplet uniformity. Critically, even at 40 °C, many formulations, particularly F3P2 and F6P2, consistently exhibited PDI values lower than 0.2 throughout storage. This result suggests that these formulations have better kinetic stability because they maintain a homogeneous droplet population. Such low PDI values are generally associated with good colloidal stability and reproducible performance [60, 73].

The formulations maintained extremely negative zeta potential values throughout all storage conditions, particularly below −40 mV. Statistical comparison between Day 1 and Month 3 showed no significant reduction in electrostatic stabilization at 5 °C and 25 °C ($p > 0.05$). At 40 °C, slight but statistically significant decreases in absolute zeta potential values were observed ($p < 0.05$), yet all systems remained within the range considered adequate for colloidal stability.

As shown in Fig. 3, both F3P2 and F6P2 maintained droplet sizes within the nanometric range, with only minor increases observed at 40 °C, while PDI values remained narrow (Fig. 4) and zeta potentials stayed within the stable range (Fig. 5). Consequently, the overall stability assessment confirmed that all formulations tested were physically stable under the studied conditions. Furthermore, the exceptional performance of F3P2 and F6P2 in maintaining small droplet sizes, uniform distribution, and strong surface charge makes them the most suitable options for further efficacy investigations.

During a three-month storage duration, the pH values of all formulations continuously varied between 5.5 and 5.9, indicating a minimal risk of irritation and compatibility with the skin's physiological surface [74]. At 40 °C, only minor reductions were observed, consistent with previously documented temperature-induced hydrolytic alterations in NE systems [38]. The ion distribution in the aqueous phase remained stable, as indicated by the minor fluctuations in conductivity values (~ 1300–1500 µS). A minor increase was noted under accelerated storage (40 °C), most likely as a result of stress-induced interfacial rearrangements, whereas values remained constant at 25 °C and 4 °C [75]. Crucially, no abrupt shifts were observed, indicating that phase separation did not occur.

Both F3P2 and F6P2 exhibited characteristic shear-thinning (pseudoplastic) behavior, with viscosity declining as the shear rate ascended (Fig. 6). This flow profile is deemed

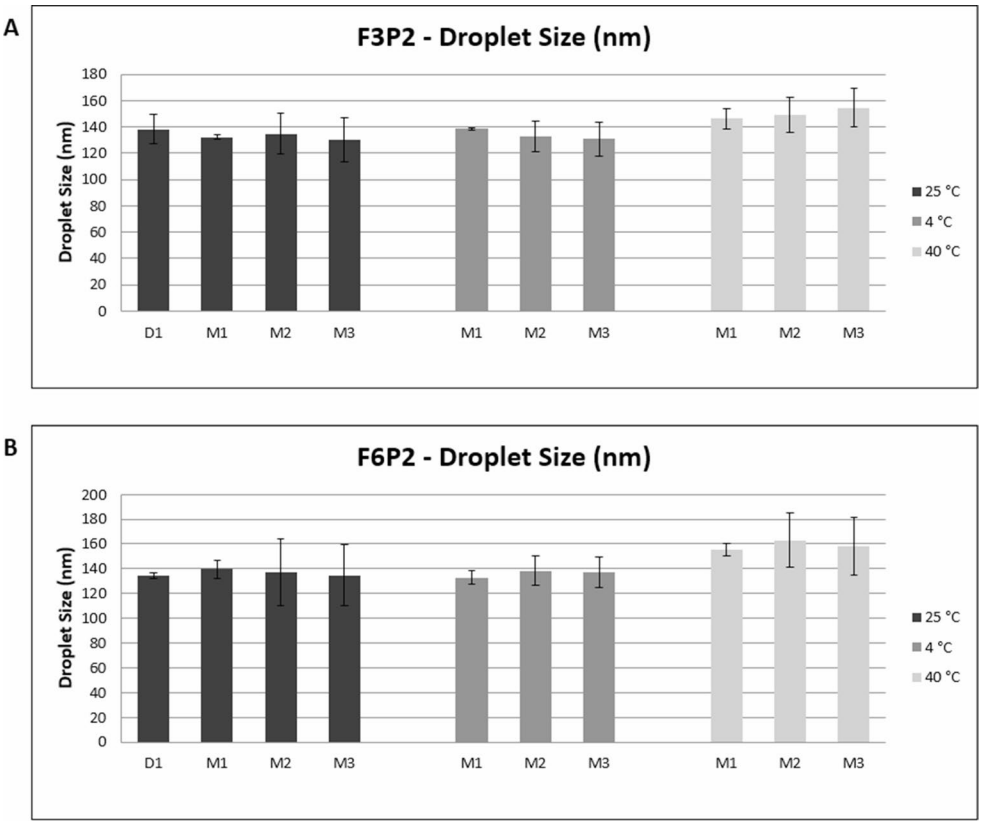


Fig. 3 Droplet size stability profiles of selected nanoemulgels (F3P2 and F6P2) under different storage conditions (25 °C, 4 °C, 40 °C) over a three-month period

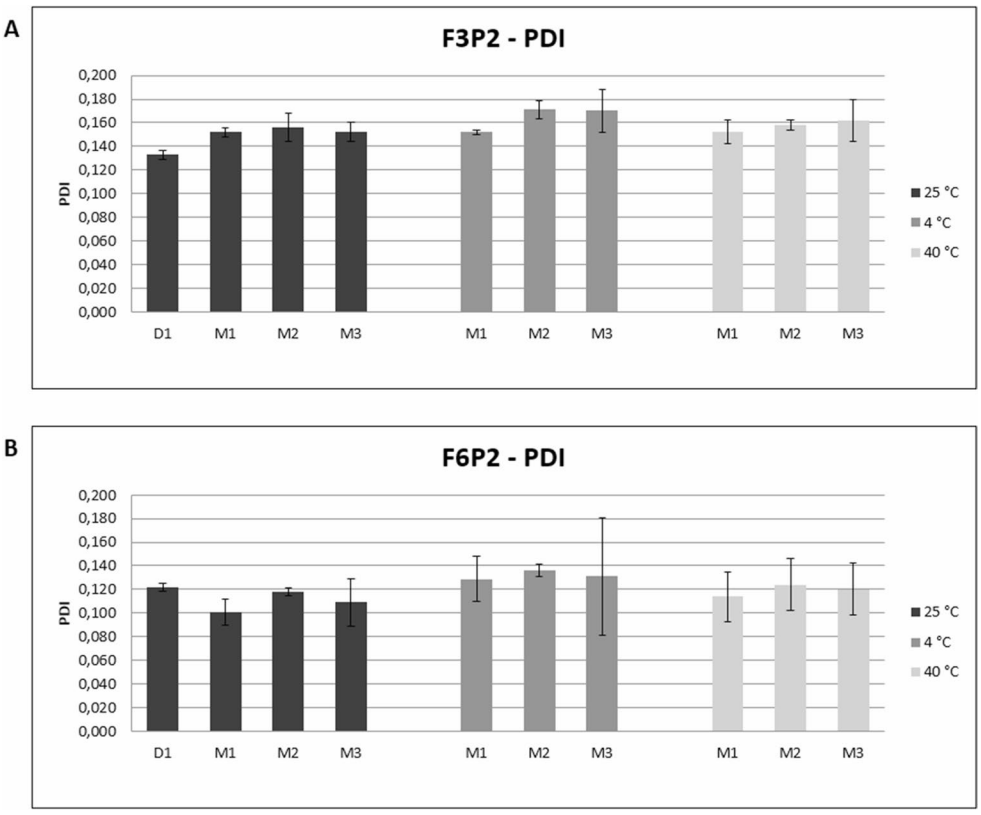


Fig. 4 PDI stability profiles of selected nanoemulgels (F3P2 and F6P2) under different storage conditions (25 °C, 4 °C, 40 °C) over a three-month period

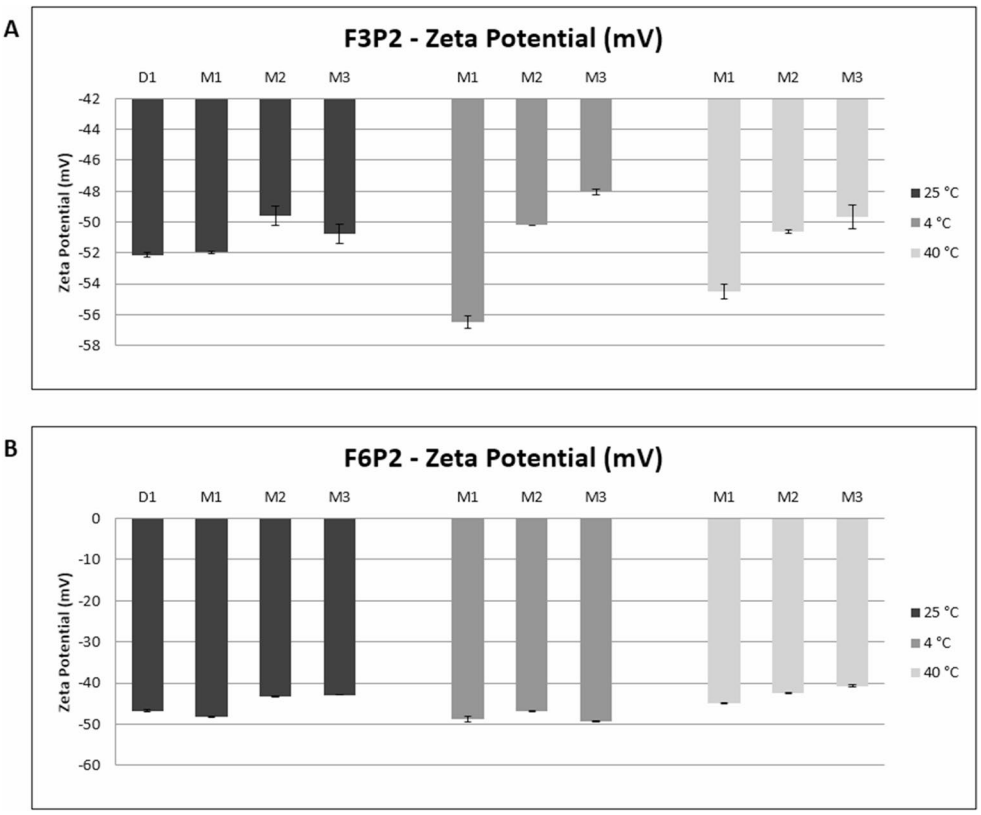


Fig. 5 Zeta potential stability profiles of selected nanoemulgels (F3P2 and F6P2) under different storage conditions (25 °C, 4 °C, 40 °C) over a three-month period

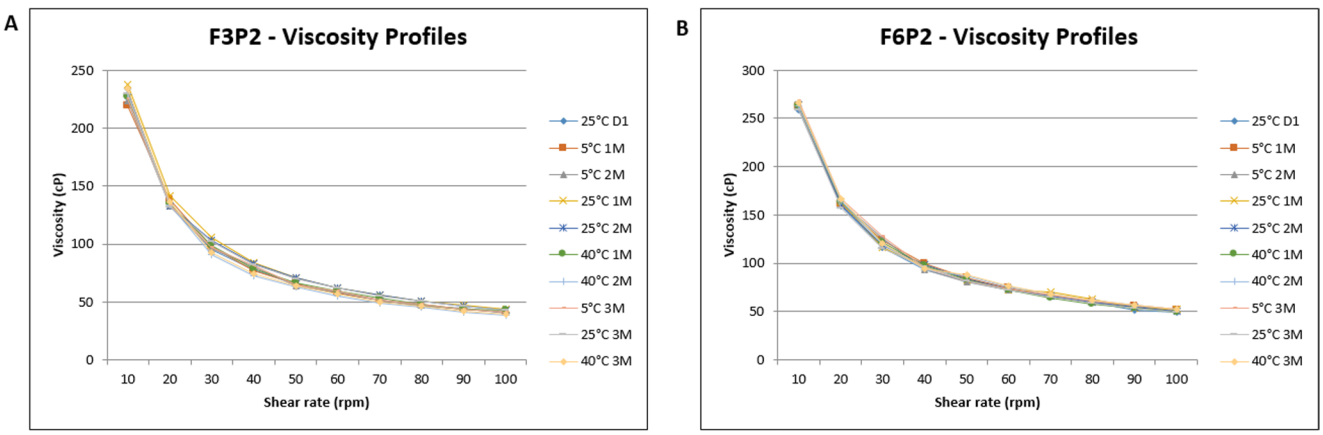


Fig. 6 Viscosity profiles of selected nanoemulgels (F3P2 and F6P2) under different storage conditions over a three-month period

beneficial for topical treatments, enhancing spreadability during application while ensuring stability at rest [76]. During the three-month storage period, viscosity readings exhibited relative stability, with only slight fluctuations and no significant time reduction, indicating robust rheological stability. Temperature, however, had a clearer impact: at 40 °C, both formulations exhibited moderate reductions in viscosity compared to samples stored at 25 °C and 4 °C, which is consistent with previous reports describing the weakening of intermolecular interactions at elevated temperatures [77]. Despite these changes, the pseudoplastic flow pattern was maintained under all tested conditions, supporting the robustness and practical applicability of the formulations.

Texture Profile Analysis

TPA was used to obtain further information on the mechanical and adhesive properties of the optimized NEG formulations. The results showed that the hardness values of F3P2 and F6P2 were in the range of 0.04–0.06 N, consistent with the values generally reported for topical hydrogel systems. Szulc-Musioł et al. (2023) reported hardness values ranging

from 0.050 to 0.065 N for quercetin-loaded sodium alginate, methylcellulose, and carboxymethylcellulose hydrogels [78]. This suggests that the hardness values found in this study are within a window that is both physiologically acceptable and supported by literature for dermal application. F6P2's slightly higher hardness (≈ 0.06 N) than F3P2's (≈ 0.04 N) indicates better spreadability combined with enough firmness to preserve structural integrity.

The adhesiveness values of both formulations (≈ 0.25 mJ) were at the upper end of the range reported in the literature (0.10–0.25 mJ) [78]. This demonstrates that NEGs can provide adequate retention on the skin surface while avoiding excessive stickiness—a balance considered desirable for periorbital and dermal application. Furthermore, adhesive strength remained moderate (~0.03–0.04 N), further confirming the positive properties during use.

The two formulations showed a marked difference in cohesiveness. F3P2 demonstrated a comparatively low cohesiveness (~ 0.57), but F6P2 displayed a markedly higher value (~ 1.77). The results position F6P2 within the cohesiveness range (1.31–2.70) established by Szulc-Musioł et al. (2023), signifying enhanced internal structural integrity and resilience to deformation [78]. This mechanical strength enhances the formulation's skin retention and facilitates the controlled release of active substances. In contrast, the diminished cohesiveness of F3P2 results in a less robust network, potentially undermining durability under mechanical stress; yet, its pliability may enhance sensory acceptance during application.

The TPA results show that both of the chosen formulations have mechanical properties that work well with topical application systems that have been described in the literature [78]. From a periocular application perspective, appropriate spreadability is essential to allow gentle distribution over the thin and highly mobile eyelid skin without excessive mechanical force [79–81]. The low hardness values (0.04–0.06 N) suggest low resistance to deformation, supporting easy application/spreadability and potentially improving user comfort in this sensitive area.

In addition, sufficient cohesiveness and moderate adhesiveness are critical to prevent dripping or migration into the ocular surface, while avoiding excessive tackiness that may cause discomfort or pulling sensation during blinking [82–84]. The mechanical profile of F6P2, characterized by balanced firmness, cohesiveness, and moderate adhesive strength, suggests a stable yet soft gel structure capable of maintaining residence on the periocular skin without undesired flow. Such properties are considered desirable for periocular dermocosmetic products, where controlled retention, non-dripping behavior, and acceptable sensory attributes are essential for user compliance and safety.

Antioxidant Activity (DPPH and ABTS Assays)

DPPH and ABTS radical scavenging assays were used to measure the antioxidant activity of the final NEGs (F3P2 and F6P2). The antioxidant capacities of the extracts, placebo systems, and NEGs are summarized in Table 4. Both formulations showed stronger antioxidant activity compared to their respective placebos (PL1 and PL2) and showed lower IC_{50} values than the individual plant extracts (*G. glabra* and *A. hippocastanum*). Among all tested samples, F6P2 exhibited comparatively higher activity, showing IC_{50} values of 22.65 µg/mL for DPPH and 10.42 µg/mL for ABTS. The lower IC_{50} values indicate enhanced radical scavenging capacity relative to crude extracts under the tested conditions.

Several factors may explain the observed improvement. First, by making poorly water-soluble phytochemicals more soluble and dispersible, the NEG system may facilitate improved interaction between antioxidant molecules and radical species. Previous studies have consistently reported improvements in the radical scavenging capacity of lipophilic antioxidants (e.g., thymol, oregano essential oil, carvacrol, and carotenoids) when encapsulated in NEs or nanocarriers as opposed to their free forms [28, 85, 86]. Furthermore, the observed potency may be attributed to the combined effects of *A. hippocastanum* phenolic components and *G. glabra* flavonoids (such as glabridin).

When the DPPH and ABTS assays were compared, the ABTS assay consistently had lower IC_{50} values. This is expected because DPPH is restricted to organic media, while $ABTS^{\bullet+}$ radicals are more reactive in both aqueous and lipophilic environments. Antioxidant screening studies have generally recognized similar assay-dependent differences [87, 88].

Table 4 Antioxidant activity (IC_{50}, µg/mL) of extracts, placebo formulations, and nanoemulgels determined by DPPH and ABTS assays (mean ± SD, $n = 3$)

Sample	DPPH (IC50, µg/mL)	ABTS (IC50, µg/mL)
G. glabra extract	34.12 ± 0.01	15.13 ± 0.10
A. hippocastanum extract	44.79 ± 0.05	14.94 ± 0.14
PL1	61.60 ± 0.06	23.50 ± 0.11
PL2	65.30 ± 0.02	30.41 ± 0.20
F3P2	26.50 ± 0.11	12.40 ± 0.19
F6P2	22.65 ± 0.08	10.42 ± 0.15
Ascorbic acid	4.12 ± 0.01	-
Trolox	-	3.21 ± 0.01

Values are expressed as mean ± SD ($n = 3$). PL1 = placebo of F3P2; PL2 = placebo of F6P2. Lower IC_{50} values indicate stronger antioxidant activity. Ascorbic acid and Trolox were used as positive controls for DPPH and ABTS assays, respectively

Additionally, placebo formulations (PL1 and PL2) also exhibited some antioxidant activity. This effect is likely due to the natural biosurfactant Quillaja saponin, which acts as an emulsifier and contains polyphenolic residues capable of scavenging radicals. According to previous studies, quillaja extracts have been found to possess natural antioxidant properties [89]. Because esterified vitamin E lacks a free hydroxyl group necessary for hydrogen donation, the addition of α-tocopheryl acetate to placebo formulations is thought to have no significant effect on radical scavenging in chemical analyses [90]. Ascorbic acid (IC_{50} = 4.12 µg/mL in DPPH) and Trolox (IC_{50} = 3.21 µg/mL in ABTS) showed the highest activities when compared to positive controls, demonstrating the assays' validity.

Although the antioxidant activity of NEGs did not reach the potency of pure reference antioxidants such as ascorbic acid and Trolox, the NEG system preserved and potentially enhanced the functional performance of the plant extracts. Importantly, the added value of nanoformulation lies not only in intrinsic radical scavenging enhancement in cell-free systems, but also in improved dispersion, physicochemical stability, and potential dermal delivery performance of phytochemicals [91–93]. These formulation-driven advantages are particularly relevant for topical applications, where stability, penetration, and residence time influence biological efficacy [91, 92].

In conclusion, F6P2 had the highest efficacy, exhibiting notable radical scavenging activity in the DPPH and ABTS assays. These findings support the potential applicability of NEG systems in pharmaceutical and cutaneous formulations where oxidative stress is a critical concern, illustrating its capacity to enhance the antioxidant efficacy of phytochemical-rich extracts.

Anti-Inflammatory (LOX Inhibition) and Anti-Tyrosinase Activity

The inhibition of lipoxygenase (LOX) was chosen as the primary anti-inflammatory test due to its crucial involvement in the synthesis of leukotrienes, which are significant mediators in the development of edema, increased vascular permeability, and intensified skin inflammation [94, 95]. LOX-driven pathways are especially pertinent in cases of hyperpigmentation and swelling, where leukotriene-induced microvascular inflammation leads to tissue darkening and fluid accumulation [96]. The reasons for selecting the LOX inhibition assay are the following: (i) it is relevant to inflammation-associated periorbital hyperpigmentation and edema in the clinic; (ii) it assesses leukotriene-related inflammatory pathways pertinent to both plant extracts; and (iii) it is a well-established in vitro method for assessing the anti-inflammatory action of bioactive phytocompounds.

Table 5 Lipoxygenase (LOX) and tyrosinase inhibition (%) of extracts, placebo formulations, and nanoemulgels at 20 µg/mL (mean ± SD, n = 3)

Sample	LOX inhibition (%)	Tyrosinase inhibition (%)
G. glabra extract	77.12 ± 0.05	69.14 ± 0.07
A. hippocastanum extract	81.2 ± 0.1	78.5 ± 0.09
PL1	23.1 ± 0.03	16.1 ± 0.06
PL2	21.83 ± 0.03	12.98 ± 0.05
F3P2	78.13 ± 0.02	71.2 ± 0.08
F6P2	80.11 ± 0.04	76.9 ± 0.03
NDGA	99.9 ± 0.01	
Kojic acid		99.8 ± 0.01

Values represent % inhibition measured at 20 µg/mL. PL1 = placebo of F3P2; PL2 = placebo of F6P2. NDGA = nordihydroguaiaretic acid, positive control for LOX; Kojic acid = positive control for tyrosinase

Based on these mechanistic considerations, the LOX inhibition assay was employed to assess whether the extracts and formulations demonstrate measurable anti-inflammatory effects. The inhibitory effects of the extracts, placebo formulations, and NEGs on LOX and tyrosinase at 20 µg/mL are summarized in Table 5. Both *G. glabra* and *A. hippocastanum* extracts showed strong LOX inhibition (77.1% and 81.2%, respectively) and notable tyrosinase inhibition (69.1% and 78.5%). These results are in line with earlier research showing that plant extracts high in phenolics have anti-inflammatory and anti-tyrosinase properties. For instance, it has been demonstrated that *G. glabra* flavonoids, such as glabridin and liquiritigenin, strongly suppress LOX and tyrosinase activity [97–99]. The anti-inflammatory properties of *A. hippocastanum* saponins and phenolics have been linked to LOX inhibitory activity [100]. The PL1 and PL2 placebo formulations, as anticipated, exhibited negligible activity (LOX inhibition of approximately 23% and 22%; tyrosinase inhibition of approximately 16% and 13%). This demonstrates that the plant extracts, not the excipients, are responsible for the effects of the designed formulations.

Oxidative stress plays a critical role in the pathogenesis of hyperpigmentation by promoting melanogenesis through the activation of key signaling pathways, including Microphthalmia-associated transcription factor (MITF) and tyrosinase expression. Increased levels of reactive oxygen species (ROS) stimulate melanocyte activity, leading to excessive melanin production and accumulation in the periorbital region [101]. Furthermore, oxidative stress is closely associated with inflammatory responses, which can further exacerbate pigmentation disorders through the release of pro-inflammatory mediators [94]. In this context, the strong antioxidant activity exhibited by the developed NEG formulations may contribute to the regulation of melanogenic processes by reducing oxidative stress and

indirectly modulating tyrosinase activity. The observed anti-inflammatory effects, as demonstrated by LOX inhibition, may also play a complementary role by attenuating inflammation-induced pigmentation pathways. Therefore, the combined antioxidant and anti-inflammatory properties of the formulations suggest a multifunctional mechanism of action potentially relevant to pigmentation-related pathways in the periorbital region.

The NEG formulations (F3P2 and F6P2) exhibited inhibition values comparable to those of the corresponding crude extracts under the tested conditions. These findings indicate that the nanoformulation preserved the intrinsic enzyme inhibitory activity of the plant extracts without functional loss. Although F6P2 exhibited numerically higher inhibition values compared to F3P2, the differences were modest under the tested conditions. Therefore, while the hybrid surfactant system may contribute to improved interfacial characteristics and dispersion of bioactive compounds, a definitive enhancement in enzyme inhibition cannot be asserted.

Limitations and Future Research

This study provides significant insights into the physicochemical properties and biological effectiveness of NEG formulations, although it is essential to acknowledge specific limitations. The biological assays conducted—antioxidant, anti-inflammatory (LOX inhibition), and anti-tyrosinase activity—were executed in vitro utilizing isolated enzyme systems. While these models offer mechanistic insights, they fail to completely represent the complex biochemical and structural milieu of human skin. As a result, the extent to which these observed activities translate into tangible clinical outcomes is yet to be determined. An additional limitation of this study is the absence of in vitro release and ex vivo skin permeation/deposition studies. Although the physicochemical properties and biological activities of the formulations suggest potential for enhanced dermal delivery, the lack of direct skin penetration data limits the ability to establish a clear correlation between the observed in vitro findings and actual skin delivery performance. Therefore, conclusions regarding dermal retention and periocular localization remain hypothetical and should be interpreted with caution. Although the enzyme inhibition results (LOX and tyrosinase assays) indicate promising biological activity, these findings are derived from simplified in vitro systems and may not fully represent the complex physiological conditions of human skin. Therefore, any interpretation regarding their effectiveness in reducing hyperpigmentation or edema in vivo should be interpreted with caution.

Another limitation is the absence of clinical evaluation. Although the formulations showed promising stability and multifunctional biological activity in vitro, their actual performance on periorbital skin—such as effects on pigmentation, vascular congestion, and edema—has not been validated. Additionally, the safety of long-term application around the sensitive periocular area needs thorough evaluation through standardized irritation and tolerability studies. Subsequent research should focus on ex vivo skin investigations, in vitro release studies, ocular-periorbital safety evaluations, and controlled clinical trials to determine the therapeutic efficacy of the formulations in humans. Furthermore, mechanistic investigations into their effects on melanogenic signaling pathways (e.g., MITF, tyrosinase expression), inflammatory mediators, and microvascular physiology would clarify the combined or complementary effects indicated by the present findings. Such studies will support the translation of NEG technologies into clinically relevant cosmetic or dermatological applications.

Conclusion

In this research, our objective was to develop NEG formulations enhanced with extracts from *G. glabra* and *A. hippocastanum* to tackle two common concerns in the periorbital area: hyperpigmentation and edema. The findings indicate that the optimized systems, notably F3P2 and F6P2, exhibit a combination of notable biological activity and physicochemical stability. Their incorporation into the gel base provided improved kinetic stability and appropriate rheological properties, while their high surface charge, narrow distribution, and nanometer-scale droplet sizes support physicochemical stability during the study period. Beyond their technical stability, the formulations also demonstrated meaningful biological performance. Both extracts contributed to the observed biological activity, leading to notable antioxidant and anti-inflammatory responses, along with measurable inhibition of tyrosinase. Although the inhibitory activity remained lower than that of the reference compound kojic acid, the results indicate that the combined formulation preserves the functional activity of the individual extracts. These findings suggest a potential multifunctional role in addressing pigmentation- and edema-related pathways, highlighting their relevance for dermocosmetic applications. Our findings offer robust in vitro evidence; however, additional studies are necessary to validate the clinical significance of these results. Future in vivo trials, followed by controlled clinical evaluations, will be critical to determine their safety, tolerability, and effectiveness in real-world use. If these outcomes are confirmed, such NEG systems may represent a promising plant-based alternative to current periorbital therapies.

Supplementary Information The online version contains supplementary material available at https://doi.org/10.1007/s12247-026-10752-2.

Author contributions E.A. conceived and designed the study. E.A., V.M., M.Y., and A.E.K. were responsible for data acquisition. Data analysis and interpretation were carried out by E.A. and A.E.K. The manuscript was drafted by E.A., and critically revised by E.A. Final approval of the version to be published and overall accountability were provided by E.A. Technical and material support were contributed by E.A. and A.E.K. Supervision of the project was performed by E.A. All authors reviewed and approved the final manuscript.

Funding Open access funding provided by the Scientific and Technological Research Council of Türkiye (TÜBİTAK).

Data Availability The datasets generated and/or analyzed during the current study are available from the corresponding author on reasonable request.

Declarations

Competing interests The authors declare no competing interests.

Open Access This article is licensed under a Creative Commons Attribution 4.0 International License, which permits use, sharing, adaptation, distribution and reproduction in any medium or format, as long as you give appropriate credit to the original author(s) and the source, provide a link to the Creative Commons licence, and indicate if changes were made. The images or other third party material in this article are included in the article's Creative Commons licence, unless indicated otherwise in a credit line to the material. If material is not included in the article's Creative Commons licence and your intended use is not permitted by statutory regulation or exceeds the permitted use, you will need to obtain permission directly from the copyright holder. To view a copy of this licence, visit http://creativecommons.org/licenses/by/4.0/.

References

1. Sarkar R, et al. Periorbital hyperpigmentation: a comprehensive review. J Clin Aesthetic Dermatol. 2016;9(1):49.
2. Samaan CB, Cartee TV. Treatment of periorbital vascularity, erythema, and hyperpigmentation. Clin Plast Surg. 2023;50(3):399–409.
3. Hamie H, et al. A review of the efficacy of popular eye cream ingredients. Int J Women's Dermatology. 2024;10(2):e156.
4. Pillaiyar T, Manickam M, Namasivayam V. Skin whitening agents: Medicinal chemistry perspective of tyrosinase inhibitors. J Enzyme Inhib Med Chem. 2017;32(1):403–25.
5. Nautiyal A, Wairkar S. Management of hyperpigmentation: Current treatments and emerging therapies. Pigment cell melanoma Res. 2021;34(6):1000–14.
6. Raina N, et al. New insights in topical drug delivery for skin disorders: from a nanotechnological perspective. ACS omega. 2023;8(22):19145–67.
7. Hajleh MNA et al. *Nanotechnology-powered cosmetics: progress in hyperpigmentation treatment.* Precis Nanomedicine. 2025; pp. 1431–1453.
8. Li C-x, et al. Pharmacological properties of glabridin (a flavonoid extracted from licorice): A comprehensive review. J Funct Foods. 2021;85:104638.
9. Sawant O, Khan T. Management of periorbital hyperpigmentation: An overview of nature-based agents and alternative approaches. Dermatol Ther. 2020;33(4):e13717.
10. Gallelli L. *Escin: A review of its anti-edematous, anti-inflammatory, and venotonic properties.* Drug design, development and therapy. 2019; pp. 3425–3437.
11. Özkan EE, et al. In vitro skin permeation of escin in the new gel formulation of Aesculus hippocastanum (Horse Chestnut). J Fac Pharm Istanbul Univ. 2016;46(2):79–88.
12. Belcaro G, et al. Evaluation of the efficacy of a new escin-based, multi-component formulation in reducing eyelid edema. Minerva Oftalmol. 2016;58:65–9.
13. Ojha B, et al. Nanoemulgel: A promising novel formulation for treatment of skin ailments. Polym Bull. 2022;79(7):4441–65.
14. Schreiner TB, et al. Formulation and optimization of nanoemulsions using the natural surfactant saponin from quillaja bark. Molecules. 2020;25(7):1538.
15. Silva CC, et al. Antioxidant and anti-tyrosinase activities of quercetin-loaded olive oil nanoemulsion as potential formulation for skin hyperpigmentation. J Dispers Sci Technol. 2023;44(14):2628–38.
16. Jacobus Berlitz S, et al. Azelaic acid-loaded nanoemulsion with hyaluronic acid–a new strategy to treat hyperpigmentary skin disorders. Drug Dev Ind Pharm. 2019;45(4):642–50.
17. Buranajaree S, et al. Depigmenting action of a nanoemulsion containing heartwood extract of Artocarpus incisus on UVB-induced hyperpigmentation in C57BL/6 mice. J Cosmet Sci. 2011;62(1):1–14.
18. Syed Azhar SNA, Ashari SE, Salim N. Development of a kojic monooleate-enriched oil-in-water nanoemulsion as a potential carrier for hyperpigmentation treatment. Int J Nanomed. 2018; pp. 6465–79.
19. Santos MO, Sequeira ML, Silva R. Is there a gold standard for treating periorbital hyperpigmentation?–A narrative review of the latest evidence. J Cutan Aesthetic Surg. 2025;18(4).
20. Shanker K, et al. RP-HPLC method for the quantitation of glabridin in Yashti-madhu (Glycyrrhiza glabra). Chromatographia. 2007;65(11):771–4.
21. Durante C, et al. Analytical concentrations of some elements in seeds and crude extracts from Aesculus hippocastanum, by ICP-OES technique. Agronomy. 2020;11(1):47.
22. Guideline I.H.T. Validation of analytical procedures: text and methodology. Q2 (R1). 2005;1(20):05.
23. Carpenter J, Saharan VK. Ultrasonic assisted formation and stability of mustard oil in water nanoemulsion: Effect of process parameters and their optimization. Ultrason Sonochem. 2017;35:422–30.
24. Leong T, et al. Minimising oil droplet size using ultrasonic emulsification. Ultrason Sonochem. 2009;16(6):721–7.
25. Nirmala MJ et al. Ultrasonic nanoemulsification of cuminum cyminum essential oil and its applications in medicine. Int J Nanomed. 2020; pp. 795–807.
26. Nirmala MJ et al. Preparation of celery essential oil-based nanoemulsion by ultrasonication and evaluation of its potential anticancer and antibacterial activity. Int J Nanomed. 2020; pp. 7651–66.
27. Yang Y, et al. Formation and stability of emulsions using a natural small molecule surfactant: Quillaja saponin (Q-Naturale®). Food Hydrocolloids. 2013;30(2):589–96.
28. Doost AS, et al. Production of thymol nanoemulsions stabilized using Quillaja Saponin as a biosurfactant: Antioxidant activity enhancement. Food Chem. 2019;293:134–43.
29. Zeng L, et al. Formation and physical stability of Zanthoxylum bungeanum essential oil based nanoemulsions co-stabilized with tea saponin and synthetic surfactant. Molecules. 2021;26(24):7464.
30. Nakmode D, et al. Fundamental aspects of lipid-based excipients in lipid-based product development. Pharmaceutics. 2022;14(4):831.

31. Osborne DW, Musakhanian J. Skin penetration and permeation properties of Transcutol®—neat or diluted mixtures. AAPS PharmSciTech. 2018;19(8):3512–33.
32. Gulcin İ. Antioxidants: a comprehensive review. Arch Toxicol. 2025; pp. 1–105.
33. Debraj D, Carpenter J, K Vatti A. Understanding the effect of the oil-to-surfactant ratio on eugenol oil-in-water nanoemulsions using experimental and molecular dynamics investigations. Ind Eng Chem Res. 2023;62(41):p16766–16776.
34. Algahtani MS, Ahmad MZ, Ahmad J. Investigation of factors influencing formation of nanoemulsion by spontaneous emulsification: impact on droplet size, polydispersity index, and stability. Bioengineering. 2022;9(8):384.
35. Liu M, et al. Garlic essential oil in water nanoemulsion prepared by high-power ultrasound: Properties, stability and its antibacterial mechanism against MRSA isolated from pork. Ultrason Sonochem. 2022;90:106201.
36. Ceylan MM. The influence of high pressure homogenization and high-intensity ultrasound on the functional properties of whey-protein/canola oil nanoemulsions during storage. Harran Tarım ve Gıda Bilimleri Dergisi. 2022;26(2):237–43.
37. Kumari S, et al. Thymol nanoemulsion exhibits potential antibacterial activity against bacterial pustule disease and growth promotory effect on soybean. Sci Rep. 2018;8(1):6650.
38. Bernardi DS, et al. Formation and stability of oil-in-water nanoemulsions containing rice bran oil: in vitro and in vivo assessments. J Nanobiotechnol. 2011;9(1):44.
39. Kotta S, et al. Formulation of nanoemulsion: a comparison between phase inversion composition method and high-pressure homogenization method. Drug Delivery. 2015;22(4):455–66.
40. Ribeiro RCdA, et al. Production and characterization of cosmetic nanoemulsions containing Opuntia ficus-indica (L.) Mill extract as moisturizing agent. Molecules. 2015;20(2):2492–509.
41. Dahake Prasanna T, et al. Formulation and physical characterization of bio-degradable chitosan-poloxamer gel base for local drug delivery. J Drug Delivery Ther. 2020;10(4):59–66.
42. Blois MS. Antioxidant determinations by the use of a stable free radical. Nature. 1958;181(4617):1199–200.
43. Re R, et al. Antioxidant activity applying an improved ABTS radical cation decolorization assay. Free Radic Biol Med. 1999;26(9–10):1231–7.
44. Baylac S, Racine P. Inhibition of 5-lipoxygenase by essential oils and other natural fragrant extracts. Int J Aromather. 2003;13(2–3):138–42.
45. Hearing VJ, Jiménez M. Mammalian tyrosinase—the critical regulatory control point in melanocyte pigmentation. Int J Biochem. 1987;19(12):1141–7.
46. Abudayeh ZHM, et al. Determination of four major saponins in skin and endosperm of seeds of horse chestnut (Aesculus hippocastanum L.) using high performance liquid chromatography with positive confirmation by thin layer chromatography. Adv Pharm Bull. 2015;5(4):587.
47. De Almeida PA, et al. New HPLC method for quality control ofβ-escin in Aesculus hippocastanum L. Hydroalcoholic extract. Lat Am J Pharm. 2013;32:1082–7.
48. Vrcek I, Ozgur O, Nakra T. Infraorbital dark circles: a review of the pathogenesis, evaluation and treatment. J Cutan aesthetic Surg. 2016;9(2):65–72.
49. Murphy MJ, Dow AA. Natural cosmeceutical ingredients for the management of hyperpigmentation in Hispanic and Latino women. J Clin Aesthetic Dermatol. 2021;14(8):52.
50. Liu J, et al. Glycyrrhiza glabra extract as a skin-whitening Agent: Identification of active components and CRTC1/MITF pathway-inhibition mechanism. J Ethnopharmacol. 2025;349:119948.
51. Giri S, et al. Formulation and evaluation of turmeric-and neem-based topical nanoemulgel against microbial infection. Gels. 2024;10(9):578.
52. Gang HZ, et al. Mixing of surfactin, an anionic biosurfactant, with alkylbenzene sulfonate, a chemically synthesized anionic surfactant, at the n-decane/water interface. J Surfactants Deterg. 2021;24(3):445–57.
53. Shah MUH, et al. A binary mixture of a biosurfactant and an ionic liquid surfactant as a green dispersant for oil spill remediation. J Mol Liq. 2019;280:111–9.
54. Musakhanian J, Osborne DW, Rodier J-D. Skin penetration and permeation properties of Transcutol® in complex formulations. AAPS PharmSciTech. 2024;25(7):201.
55. Algahtani MS, Ahmad MZ, Ahmad J. Nanoemulgel for improved topical delivery of retinyl palmitate: formulation design and stability evaluation. Nanomaterials. 2020;10(5):848.
56. Halla N, et al. Cosmetics preservation: a review on present strategies. Molecules. 2018;23(7):1571.
57. Iwasaki T, Uchiyama R, Nosaka K. Difference in anti-microbial activity of propan-1, 3-diol and propylene glycol. Chem Pharm Bull. 2023;71(1):74–7.
58. Pinto JR, Monteiro e SA, Silva, Leonardi GR. Effects of 1, 3-propanediol associated, or not, with butylene glycol and/or glycerol on skin hydration and skin barrier function. Int J Cosmet Sci. 2024;46(1):85–95.
59. Park YH, Shin J, Kim HJ. Effect of α-tocopherol on the oxidative stability of horse oil-in-water emulsion during storage. Food Sci Biotechnol. 2023;32(5):639–45.
60. Gupta A, et al. Nanoemulsions: formation, properties and applications. Soft Matter. 2016;12(11):2826–41.
61. Rajasekaran B, et al. Shrimp oil nanoemulsions prepared by microfluidization and ultrasonication: characteristics and stability. RSC Adv. 2024;14(9):6135–45.
62. Mirković D, Ibrić S. Investigation of short-term stability of parenteral nutrition nanoemulsions prepared under laboratory conditions. Vojnosanit Pregl. 2020;77(7):688–96.
63. Banerjee A, et al. Synthesis, characterization and stress-testing of a robust quillaja saponin stabilized oil-in-water phytocannabinoid nanoemulsion. J cannabis Res. 2021;3(1):43.
64. Wooster TJ, Golding M, Sanguansri P. Impact of oil type on nanoemulsion formation and Ostwald ripening stability. Langmuir. 2008;24(22):12758–65.
65. L'estimé M, et al. Droplet size distribution in emulsions. Langmuir. 2023;40(1):275–81.
66. Zhu Z, et al. Comparison of natural and synthetic surfactants at forming and stabilizing nanoemulsions: Tea saponin, Quillaja saponin, and Tween 80. J Colloid Interface Sci. 2019;536:80–7.
67. Abruzzo A, et al. Development and characterization of azithromycin-loaded microemulsions: a promising tool for the treatment of bacterial skin infections. Antibiotics. 2022;11(8):1040.
68. Jamshaid U, et al. Novel hydrogels based on the nano-emulsion formulation process: development, rheological characterization, and study as a drug delivery system. Pharmaceutics. 2024;16(6):812.
69. Xu M, Wan Z, Yang X. Recent advances and applications of plant-based bioactive saponins in colloidal multiphase food systems. Molecules. 2021;26(19):6075.
70. Schreiner TB, et al. Saponins as natural emulsifiers for nanoemulsions. J Agric Food Chem. 2022;70(22):6573–90.
71. Sun H, et al. Stabilization of flaxseed oil nanoemulsions based on flaxseed gum: Effects of temperature, pH and NaCl on stability. Lwt. 2023;176:114512.
72. Saab M, Raafat K, El-Maradny H. Transdermal delivery of capsaicin nanoemulgel: Optimization, skin permeation and in vivo activity against diabetic neuropathy. Adv Pharm Bull. 2021;12(4):780.
73. Danaei M, et al. Impact of particle size and polydispersity index on the clinical applications of lipidic nanocarrier systems. Pharmaceutics. 2018;10(2):57.

74. Lambers H, et al. Natural skin surface pH is on average below 5, which is beneficial for its resident flora. Int J Cosmet Sci. 2006;28(5):359–70.
75. Zhang W, et al. Electrical conductivity and stability of O/W emulsions. Acta Petrolei Sinica. 2008;24:592.
76. Eid AM, et al. Development of Vitis vinifera nanoemulgel and evaluation of its potential anticancer, antimicrobial and anti-inflammatory. BMC Complement Med Ther. 2025;25(1):47.
77. Iacob-Tudose ET, Mamaliga I, Iosub AV. TES nanoemulsions: a review of thermophysical properties and their impact on system design. Nanomaterials. 2021;11(12):3415.
78. Szulc-Musioł B, Siemiradzka W, Dolińska B. Formulation and evaluation of hydrogels based on sodium alginate and cellulose derivatives with quercetin for topical application. Appl Sci. 2023;13(13):7826.
79. Pratchyapruit W, et al. Functional analyses of the eyelid skin constituting the most soft and smooth area on the face: contribution of its remarkably large superficial corneocytes to effective water-holding capacity of the stratum corneum. Skin Res Technol. 2007;13(2):169–75.
80. Al-Smadi K, et al. Advances in characterization of transdermal and topical products using texture analyzer systems. AAPS PharmSciTech. 2025;26(5):157.
81. Al-Barghouthy EY, et al. Comparative evaluation of spreadability measurement methods for topical semisolid formulations/a scoping review. Gels. 2025;11(12):1006.
82. Goto T, et al. Cosmetic product migration onto the ocular surface: exacerbation of migration after eyedrop instillation. Cornea. 2010;29(4):400–3.
83. Wang M. J <>Craig 2018 Investigating the effect of eye cosmetics on the tear film: current insights. Clin Optom (Auckl) 10 33–40 Published online, 2018.
84. Wang MT, Craig JP. Investigating the effect of eye cosmetics on the tear film: current insights. Clin optometry, 2018: pp. 33–40.
85. da Silva BD et al. *Antioxidant, antibacterial and antibiofilm activity of nanoemulsion-based natural compound delivery systems compared with non-nanoemulsified versions.* Foods. 2023;12(9):1901.
86. Sun MZ, et al. The effect of multilayer nanoemulsion on the In Vitro digestion and antioxidant activity of β-carotene. Antioxidants. 2024;13(10):1218.
87. Bibi Sadeer N, et al. The versatility of antioxidant assays in food science and safety—Chemistry, applications, strengths, and limitations. Antioxidants. 2020;9(8):709.
88. Wołosiak R, et al. Verification of the conditions for determination of antioxidant activity by ABTS and DPPH assays—A practical approach. Molecules. 2021;27(1):50.
89. Tippel J, et al. Composition of Quillaja saponin extract affects lipid oxidation in oil-in-water emulsions. Food Chem. 2017;221:386–94.
90. Di Mambro VM, et al. Comparison of antioxidant activities of tocopherols alone and in pharmaceutical formulations. Int J Pharm. 2003;262(1–2):93–9.
91. Donthi MR, et al. Nanoemulgel: a novel nano carrier as a tool for topical drug delivery. Pharmaceutics. 2023;15(1):164.
92. Mohammadi-Samani S, et al. Oxybutynin-nanoemulgel formulation as a successful skin permeation strategy: in-vitro and ex-vivo evaluation. Front Mater. 2022;9:848629.
93. Choudhury H, et al. Recent update on nanoemulgel as topical drug delivery system. J Pharm Sci. 2017;106(7):1736–51.
94. Funk CD. Prostaglandins and leukotrienes: advances in eicosanoid biology. Science. 2001;294(5548):1871–5.
95. Samuelsson B. Leukotrienes: mediators of immediate hypersensitivity reactions and inflammation. Science. 1983;220(4597):568–75.
96. Markiewicz E et al. *Post-inflammatory hyperpigmentation in dark skin: molecular mechanism and skincare implications.* Clinical, cosmetic and investigational dermatology. 2022; pp. 2555–2565.
97. Chandrasekaran C, et al. Dual inhibitory effect of Glycyrrhiza glabra (GutGard™) on COX and LOX products. Phytomedicine. 2011;18(4):278–84.
98. Chen J, Yu X, Huang Y. Inhibitory mechanisms of glabridin on tyrosinase. Spectrochim Acta Part A Mol Biomol Spectrosc. 2016;168:111–7.
99. Noor SU, Faridah F, Michico M. Formulation of liquorice root extract (Glycyrrhiza glabra L.) as skin whitening cream. Indonesian J Plant Med. 2016;9(2):93–9.
100. Sharipov A, et al. Hypoglycemic and anti-inflammatory effects of triterpene glycoside fractions from Aeculus hippocastanum seeds. Molecules. 2021;26(13):3784.
101. Kim N-H, Lee A-Y. Oxidative stress induces skin pigmentation in melasma by inhibiting hedgehog signaling. Antioxidants. 2023;12(11):1969.

Publisher's Note Springer Nature remains neutral with regard to jurisdictional claims in published maps and institutional affiliations.